Removal of poly- and perfluoroalkyl substances (PFAS) from water by adsorption: Role of PFAS chain length, effect of organic matter and challenges in adsorbent regeneration

Journal Pre-proof

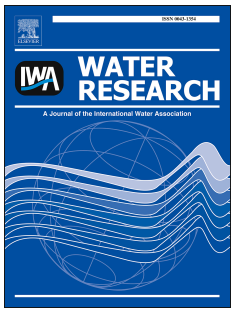

Removal of poly- and perfluoroalkyl substances (PFAS) from water by adsorption: Role of PFAS chain length, effect of organic matter and challenges in adsorbent regeneration

Erica Gagliano, Massimiliano Sgroi, Pietro P. Falciglia, Federico G.A. Vagliasindi, Paolo Roccaro

PII: S0043-1354(19)31155-8

DOI: https://doi.org/10.1016/j.watres.2019.115381

Reference: WR 115381

To appear in: *Water Research*

Received Date: 15 August 2019

Revised Date: 29 November 2019

Accepted Date: 7 December 2019

Please cite this article as: Gagliano, E., Sgroi, M., Falciglia, P.P., Vagliasindi, F.G.A., Roccaro, P., Removal of poly- and perfluoroalkyl substances (PFAS) from water by adsorption: Role of PFAS chain length, effect of organic matter and challenges in adsorbent regeneration, *Water Research* (2020), doi: https://doi.org/10.1016/j.watres.2019.115381.

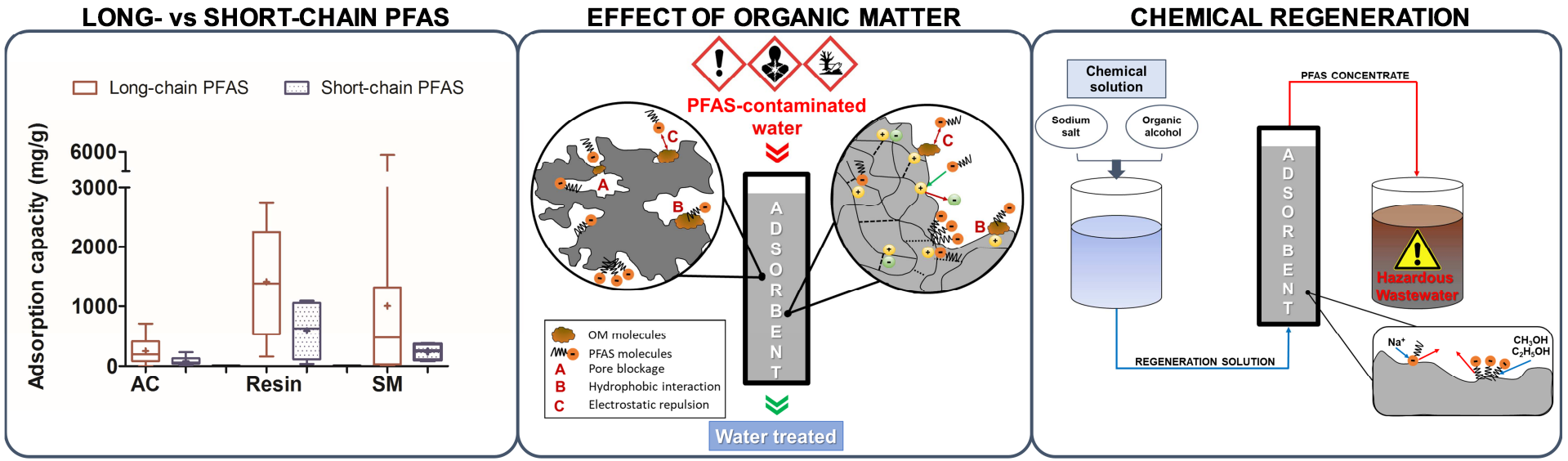

Removal of poly- and perfluoroalkyl substances (PFAS) from water by adsorption: role of PFAS chain length, effect of organic matter and challenges in adsorbent regeneration

Erica Gagliano[a], Massimiliano Sgroi[a], Pietro P. Falciglia[a,b], Federico G. A. Vagliasindi[a], Paolo Roccaro[a*]

[a] *Department of Civil Engineering and Architecture, University of Catania, Viale A. Doria 6, Catania, Italy*

[b] *Laboratori Nazionali del Sud – Istituto Nazionale di Fisica Nucleare, Via S. Sofia, 62, 95125, Catania, Italy*

**Corresponding author. Department of Civil Engineering and Architecture, University of Catania, Viale A. Doria 6, Catania, Italy*

E-mail address: paolo.roccaro@unict.it (P. Roccaro)

Abstract

Poly- and perfluoroalkyl substances (PFAS) are a wide group of environmentally persistent organic compounds of industrial origin, which are of great concern due to their harmful impact on human health and ecosystems. Amongst long-chain PFAS, perfluorooctanoic acid (PFOA) and perfluorooctane sulfonic acid (PFOS) are the most detected in the aquatic environment, even though their use has been limited by recent regulations. Recently, more attention has been posed on the short-chain compounds, due to their use as an alternative to long-chain ones, and to their high mobility in the water bodies. Therefore, short-chain PFAS have been increasingly detected in the environmental compartments. The main process investigated and implemented for PFAS removal is adsorption. However, to date, most adsorption studies have focused on synthetic water.

The main objective of this article is to provide a critical review of the recent peer-reviewed studies on the removal of long- and short- chain PFAS by adsorption. Specific objectives are to review 1) the performance of different adsorbents for both long- and short-chain PFAS, 2) the effect of organic matter, and 3) the adsorbent regeneration techniques. Strong anion-exchange resins seem to better remove both long- and short-chain PFAS. However, the adsorption capacity of short-chain PFAS is lower than that observed for long-chain PFAS. Therefore, short-chain PFAS removal is more challenging. Furthermore, the effect of organic matter on PFAS adsorption in water or wastewater under real environmental conditions is overlooked. In most studies high PFAS levels have been often investigated without organic matter presence. The rapid

breakthrough of PFAS is also a limiting factor and the regeneration of PFAS exhausted adsorbents is very challenging and needs more research.

Keywords:

Adsorption; anion-exchange; Long- and short- chain PFAS; organic matter; regeneration; adsorption mechanism.

Contents

75

76 List of abbreviations

Main PFAS and alternative compounds

F-53B	Potassium salt of 6:2 chlorinated polyfluorinated ether sulfonate
FOSA	Perfluorooctane sulfonamide
PFAS	Poly- and perfluoroalkyl substances
PFCAs	Perfluoroalkyl carboxylic acids
PFSAs	Perfluoroalkane sulfonates
PFBA	Perfluorobutanoic acid
PFBS	Perfluorobutane sulfonic acid
PFDA	Perfluorodecanoic acid
PFDoDA	Perfluorododecanoic acid
PFDS	Perfluorodecane sulfonic acid
PFHpA	Perfluoroheptanoic acid
PFHpS	Perfluoroheptane sulfonic acid
PFHxA	Perfluorohexanoic acid
PFHxS	Perfluorohexane sulfonic acid
PFNA	Perfluorononanoic acid
PFNS	Perfluorononane sulfonic acid
PFOA	Perfluorooctanoic acid
PFOS	Perfluorooctane sulfonic acid
PFPeA	Perfluoropentanoic acid
PFPeS	Perfluoropentane sulfonic acid
PFTrDA	Perfluorotridecanoic acid
PFUnDA	Perfluoroundecanoic acid

77

Adsorbent materials

2-MNPs@FG	Magnetic-nanoparticles attached into fluorographene (mass ratio of MNPs and FG is 3:5)
AC	Activated carbon
ACF	Activated carbon fiber
ARH	Aminated rice husk
BdAC	Bamboo-derived AC
CTF	Covalent triazine-based framework
DFB-CDP	Cross-linked polymer network where β-Cyclodentrix substitutes decafluorobiphenyl (DFB)
Fe_3O_4 NP	Magnetite nanoparticles
Fe_3O_4@SiO_2-NH_2&F_{13}	Silica membrane functionalized with amino group and octyl-perfluorinated chain on the Fe_3O_4 NP surface
GAC	Granular activated carbon
h-BNs	Porous hexagonal boron nitride nanosheets
HDPE	High-density polyethylene

HMS	Hexagonal mesoporous silica
HWC	Hardwood biochar
MIMs	Macromolecular imprinted materials
MIP-CMs	Molecularly imprinted carbon microspheres
MWNT	Multi-walled carbon nanotubes
NIP-CMs	Non-imprinted carbon microspheres
OD-HMS	N-octyldichlorosilane grafted hexagonal mesoporous silica
PAC	Powdered activated carbon
PACFs	Polyacrylonitrile fiber (PANF)-derived activated carbon fibers
PAF-45	Porous aromatic framework constructed from benzene rings
PCMAs	Permanently confined micelle arrays
PEI-f-CMC	Poly(ethylenimine)-functionalized cellulose microcrystals
PS	Polystyrene
PS-COOH	Poly-styrene carboxylic acid
PWC	Pinewood biochar
R-CAC	Reactivated coconut shell-based AC
SWNT	Single walled carbon nanotubes

78

Other

AE	Anion-exchange
AFFF	Aqueous fil-forming foam
AOPs	Advanced oxidation processes
ATRP	Atom transfer radical polymerization
BET	Brunauer, Emmett and Teller
BSA	Bovine serum albumin
DBP	Disinfection by-products
DI	Deionized water
DMC	Methacryloyloxyethyl trimethyl ammonium chloride
DOC	Dissolved organic carbon
DOM	Dissolved organic matter
DW	Drinking water
DWTPs	Drinking water treatment plants
EBCT	Empty bed contact time
EfOM	Effluent organic matter
EWTP	Electroplating WWTP
FA	Fulvic acids
GW	Groundwater
HA	Humic acids
LW	Lake water
MB	Methylbenzene

MPLs	Microplastics
OM	Organic matter
NDMA	N-Nitrosodimethylamine
NOM	Natural organic matter
NPs	Nanoparticles
PFSOF WWW	Perfluorooctanesulfonyl fluoride washing wastewater
RSSCT	Rapid small-scale column tests
RW	River water
S_{BET}	BET surface area
SDS	Sodium dodecyl sulphate
SeaW	Seawater
$SUVA_{254}$	Specific ultra-violet absorbance at 254 nm
SW	Surface water
TCE	Tri-chloroethylene
TEM	Transmission electron microscopy
TMFA	2-(trifluoromethyl)acrylic acid
TOC	Total organic carbon
WW	Wastewater
WWTPs	Wastewater treatment plants

79

80

1. Introduction

1.1. PFAS classification

Poly- and perfluoroalkyl substances (PFAS) are a large group of anthropogenic aliphatic compounds that are of increasing concern worldwide due to their impact on environment and human health. For many decades, they have been used in an array of formulations as surfactants intermediates (i.e., firefighting foams, hydraulic fluids for aircrafts), waterproofing treatment for textiles (i.e., apparel, carpet) and household products (i.e., paper and non-stick cookware coating) (Buck et al., 2011; Rahman et al., 2014; Xiao, 2017). PFAS contamination is the result of consumer-product degradation, firefighting activities and discharges of fluorochemical manufacturing facilities (Hu et al., 2016).

PFAS are made up of a chain of varying carbon length, on which at least one (polyfluoroalkyl acids) or all (perfluoroalkyl acids) of the hydrogen atoms bound to carbon-chain in the nonfluorinated substances have been replaced by fluorine atoms (Buck et al., 2011). Their chemical structure also includes a charged functional group commonly carboxylic or sulfonic acids attached at one end. Polyfluoroalkyl acids have also been indicated as “precursors” of perfluoroalkyl ones, hence the non-fluorinated bond provides a biotic or abiotic degradation pathway (ITRC, 2017). Depending on their terminal functional group, PFAS can be distinguished in perfluoroalkyl carboxylic acids (PFCAs) and in perfluoroalkyl sulfonic acids (PFSAs) (Buck et al., 2011). However, an abridged way to distinguish among PFAS subclasses is that referred to carbon-chain length. According to the Organization for Economic Co-operation and Development (OECD), the term “long-chain compound” indicates PFCAs with eight or more carbons, and PFSAs with six or more carbons. Whereas, “short-chain” is related to PFCAs with

seven or fewer carbons and PFSAs with five or fewer carbons (OECD/UNEP Global PFC Group, 2013). It should be noted that PFCAs and PFSAs classification, based on chain length, is different in terms of number of carbon atoms. However, PFAS bioaccumulation and biomagnification into biota increase with the increasing of carbon-chain length, PFSAs are more bioaccumulate than PFCAs with the same chain length (Ahrens, 2011).

1.2. PFAS properties

The knowledge of PFAS physical and chemical properties is paramount to understand their fate and transport in the environment. The C-F bound is the strongest covalent bond in organic chemistry and it leads to PFAS thermal stability (ITRC, 2017). In addition, PFAS exhibit mutually hydrophobic and lipophobic properties, which are primarily attributed to the low polarizability of fluorine atoms. Moreover, the terminal functional group attached to fluoroalkyl chain provides PFAS chemical stability. With the increasing replacement of hydrogen by fluorine as well as the increasing carbon-chain length, PFAS become more chemically inert. On the contrary, their water solubility increases with the decreasing carbon-chain length (Kucharzyk et al., 2017). PFCAs and PFSAs are characterized by a low vapour pressure, which makes air stripping an unsuitable technique for PFAS removal (Rahman et al., 2014). With the increasing C-F chain length, PFAS become more lipophilic as demonstrated by octanol/water partition coefficients (K_{ow}). At environmentally relevant pH, PFAS exhibit anionic species according to their low values of acid dissociation constant (pK_a). Other properties, such as resistance to thermal, biological and chemical degradation and redox stability, impart unique features to PFAS, making them suitable for several industrial applications. Information regarding chemical formulas and Chemical Abstracts Service (CAS) of

129 selected per-fluoroalkyl substances along with their physical and chemical properties
130 are reported in Table 1.

131 1.3. Occurrence of PFAS in water

132 In the aquatic environment, PFAS have been detected at low concentrations ranging
133 from pg L^{-1} to µg L^{-1} (Kaboré et al., 2018; Rahman et al., 2014) and long-chain
134 compounds, such as perfluorooctane sulfonic acid (PFOS) and perfluorooctanoic acid
135 (PFOA), are the most commonly measured PFAS around the world (ITRC, 2017).
136 Widespread occurrence of PFAS in urban water cycle including wastewater (WW), river
137 water (RW), lake water (LW), drinking water (DW), stormwater, and groundwater (GW)
138 has been demonstrated by several studies (Appleman et al., 2014; Arvaniti and
139 Stasinakis, 2015; Ateia et al., 2019; Hölzer et al., 2009; Munoz et al., 2017; Rahman et
140 al., 2014). The amount of PFAS not removed in wastewater treatment plants (WWTPs)
141 and, consequently, released into the receiving environment is a concern for the possible
142 presence of these compounds in water used for potable supply production.
143 A recent research suggests that the possible impacts of PFAS on GW is linked to the
144 use of treated WW for irrigation (Szabo et al., 2018). The occurrence and distribution of
145 PFAS remain not completely identified, due to the limited data about the removal
146 efficiency of conventional water treatment plants and about the transformation of PFAS
147 precursor compounds (Appleman et al., 2014; Arvaniti and Stasinakis, 2015).
148 Although the use of PFOS and PFOA has been reduced due to their health impact, the
149 total amount of PFAS introduced into the environment has not been reduced because
150 the long-chain compounds have been replaced by short and ultra-short PFAS (Ateia et
151 al., 2019). The latter are potentially less bioaccumulated and bioconcentrated through

trophic levels as compared to long-chain but they are still environmentally persistent (Brendel et al., 2018; OECD/UNEP Global PFC Group, 2013).

1.4. PFAS toxicity

PFAS are absorbed in human body after oral ingestion, they are not metabolized and they are detected in human tissue and blood serum at typical concentrations of ng mL^{-1}. Long-chain PFAS are taken up and stored preferentially in the liver. Half-life values of PFOS and PFOA in humans range from 2.3 to 5.4 years (Hölzer et al., 2009; Stubleski et al., 2017). Epidemiological studies have shown that the occurrence of PFOA and PFOS in humans is probably linked to a high incidence of thyroid disease, high cholesterol, ulcerative colitis, kidney cancer, testicular cancer, and pregnancy-induced hypertension (Crawford et al., 2017; Domingo and Nadal, 2017). More details concerning PFAS toxicological properties are reported in literature (Dewitt, 2015).

Based on WHO's recommendation and on the precautionary principle, the proposal for a recast of the Drinking Water Directive (98/83/CE, Directive on the quality of water intended for human consumption) published on 1st February 2018, has included the group of poly- and perfluoroalkyl substances in the list of regulated chemicals. The proposal recommends the values of 0.5 µg L^{-1} for the total amount of PFAS and 0.1 µg L^{-1} for each single compound. In 2017, the Veneto Region (Italy) set drinking water quality standards for PFAS (Veneto Legislation 1590/201), with a limit value of 90 ng L^{-1} for PFOA and PFOS (with PFOS < 30 ng L^{-1}), and a limit value of 300 ng L^{-1} for the other PFAS (sum of PFBA, PFPeA, PFBS, PFHxA, PFHpA, PFHxS, PFNA, PFDeA, PFUnA, PFDoA). Such regulation came after a large contamination of surface water and GW due to industrial WW discharges, with the subsequent bioaccumulation of

PFAS in the serum of the exposed population. As a result, PFAS are emerging contaminants already regulated in Italy.

1.5. PFAS removal

Conventional treatment processes are ineffective for PFAS degradation due to the high straight of the covalent C-F bond of their chain, their low concentration in water and their high hydrophilicity (Rahman et al., 2014; Ross et al., 2018). Biological treatment both aerobic and anaerobic are only able to break the C-C bond, and they lead to the formation of short-chain PFAS. When advanced treatment technologies are not implemented, biological WWTPs affect the receiving water bodies and the concentration of PFAS detected in finished water is often higher than in the untreated water (Arvaniti and Stasinakis, 2015; Kaboré et al., 2018). This fact gives evidence to recalcitrant behaviour of PFAS to biological treatment and, consequently, their formation via biodegradation of precursor compounds (Rahman et al., 2014). According to data obtained from monitoring studies, PFAS with long carbon-chain, such as PFOS, tend to accumulate in sludge, whereas perfluorobutane sulfonic acid (PFBS) has been mainly detected in the effluents of WWTPs and in drinking water treatment plants (DWTPs) (Arvaniti and Stasinakis, 2015; Rahman et al., 2014).

Under typical water treatment plant conditions, disinfection by free chlorine or UV irradiation are ineffective (Appleman et al., 2014; Rahman et al., 2014). PFAS are also much more resistant than other micro-contaminants to the oxidation by ozone and hydroxyl radicals due to the strong C-F bond and the electron withdrawing of their functional groups (Nzeribe et al., 2019; Trojanowicz et al., 2018). Furthermore, advanced oxidation processes (AOPs) often result in a partial degradation of PFAS,

198 with formation of PFAS with shorter perfluorinated alkyl chain (Nzeribe et al., 2019;
199 Trojanowicz et al., 2018).
200 Adsorption, anion-exchange (AE), high pressure nanofiltration and reverse osmosis
201 membrane processes are effective for substantial PFAS removal (Appleman et al.,
202 2013; Du et al., 2014; Kucharzyk et al., 2017).
203 Main issues inherent with PFAS removal through these mentioned techniques are the
204 influence of water matrix (i.e., competing anions, organic matter), frequent regeneration
205 (due to fast breakthrough), and disposal of concentrate with high PFAS concentration
206 (Appleman et al., 2013; Rahman et al., 2014; Zaggia et al., 2016).
207 Adsorption is actually an established technology for PFAS removal, both as single
208 process of point-of-use applications and as step of water treatment plants (Arvaniti and
209 Stasinakis, 2015; Eschauzier et al., 2012; Quiñones and Snyder, 2009). Moreover, it
210 shows a more economical performance compared to high pressure membrane
211 processes (Rizzo et al., 2019; Roccaro et al., 2013).
212 As previously mentioned, PFAS exist as anions at ambient pH values and this makes
213 strong base AE resins suitable for their removal. However, AE treatment efficiency
214 depends on the resin properties, including porosity, functional group and polymer matrix
215 (Deng et al., 2010).
216 To date, adsorption studies have addressed single long-chain PFAS (i.e., PFOA and
217 PFOS), even though long- and short-chain co-removal requires further investigation
218 (Ateia et al., 2019; Maimaiti et al., 2018; McCleaf et al., 2017). Moreover, many
219 compounds, commonly present in water bodies, could affect adsorption efficiency and

additional studies should regard their potential competition (Ateia et al., 2019; Du et al., 2015, 2014; Yu et al., 2012).

2. PFAS adsorption and scope of the review

2.1. PFAS adsorption mechanism

Electrostatic and hydrophobic interactions are considered the predominant forces that govern adsorption of PFAS on several adsorbent materials. Other less important mechanisms of PFAS adsorption are hydrogen bonding and covalent bonding. PFAS molecular structure, adsorbent chemistry and physical properties (i.e., surface functional groups, polarity, and porosity), as well as liquid phase composition should be considered as the main factors affecting PFAS adsorption efficiency (Du et al., 2014).

Electrostatic interactions occur between anionic PFAS and adsorbent material positively charged. Consequently, any changes in ionic strength (i.e., co-existing inorganic anions and changing solution pH) could affect adsorption efficiency, due to electrostatic repulsions (Du et al., 2014). Change in solution pH has an effect on the charge characteristics of PFAS molecules and surface properties of adsorbents (Liu et al., 2018; Yu et al., 2008). As reported in several studies, an increase in pH solution led to a decrease in adsorption capacity of most adsorbents (Deng et al., 2010; Gao et al., 2017; Qian et al., 2017). Nevertheless, an increase of ionic strength ascribed to the presence of monovalent and divalent cations (i.e., Na^{+}, K^{+}, Ca^{2+}, Mg^{2+}) might enhance the PFAS removal due to the compression of the electrical double layer (Du et al., 2014; Xiao et al., 2011). The salting-out effect should be also mentioned as reported in previous studies (Carter and Farrell, 2010; Chen et al., 2016). This effect occurs at high salt concentrations and it involves a decline of PFAS solubility and, consequently, their adsorption on adsorbent surface could be encouraged (Du et al., 2014). It is clear that

the presence of inorganic anions (i.e., Cl^- and SO^{4-}) involves a competition with PFAS for adsorption sites (Deng et al., 2010; Gao et al., 2017). However, the worsening of PFAS removal occurred when solution pH was higher than point of zero charge of the adsorbents, due to the establishment of electrostatic repulsions (Chen et al., 2017; Zhou et al., 2009).

Electrostatic repulsions between anions PFAS and negatively charged surfaces can be overcome through hydrophobic interactions of fluorinated chain (Zaggia et al., 2016). Moreover, removal efficiency of individual PFAS into adsorbent materials depends on the compound functional groups and C-F chain length. In detail, PFSAs are removed better than PFCAs, and long-chain compounds with the same functional group are more efficiently removed than short-chain ones (Appleman et al., 2014; Du et al., 2014; McCleaf et al., 2017; Xiao et al., 2011; Zaggia et al., 2016).

Hydrophobic effect has been found to increase with the increasing C-F chain length (Du et al., 2014; McCleaf et al., 2017; Rahman et al., 2014). This was also demonstrated in a prior work that investigated the competitive adsorption among PFAS with different chain length on kaolinite (Xiao et al., 2011). The authors argued that, due to a stronger hydrophobic interaction with the tested adsorbent, the longer-chained PFAS outcompeted the shorter during adsorption. Based on PFAS functional group, the presence of one more C-F bond in PFSAs compared to corresponding PFCAs results in stronger hydrophobic properties and increasing adsorption of PFSAs (Chen et al., 2016; Zaggia et al., 2016). Moreover, strong hydrophobic interactions favour the formation of molecular aggregates during PFOA and PFOS removal, while highly hydrophilic compounds, such as PFBA and PFBS, are removed as single molecules on adsorbent

active sites (Du et al., 2014). Exceeding the critical micelle concentration (c.m.c) may lead to the formation of multilayer structures (i.e., micelles and hemi-micelles) on adsorbent surfaces that may play an important role in PFAS adsorption (Appleman et al., 2014; Deng et al., 2013; Du et al., 2014). However, at the PFAS environmental level the formation of micelles is unlikely and only aggregates have been observed (Zaggia et al., 2016). McCleaf et al. (2017) reported that PFAS adsorption process may include two distinct phases. Initially removal occurs through PFAS adsorption on open sites of adsorbents, gradually pore sites become clogged and removal becomes a function of molecular aggregation of PFAS (McCleaf et al., 2017).

Since electrostatic negativity is originated from PFAS functional head and hydrophobic interaction is linked to C-F chain, the electrostatic interactions seem to be dominant for short-chain PFAS, while longer PFAS are adsorbed through hydrophobic interactions, which favour the formation of molecular aggregate on the active surface (Deng et al., 2012; Du et al., 2014; Zaggia et al., 2016).

2.2. Scope of the review

An important limitation of prior research on PFAS adsorption is that the evaluation of adsorption efficiency has been explored at high PFAS concentrations, which are not representative of the environmental concentration level. Furthermore, very high doses of adsorbents have been used which do not reflect the actual water treatment plant adsorption processes (Rahman et al., 2014).

Another relevant limitation of prior researches is that the experiments have often been carried out by using deionized water (DI) spiked with selected PFAS, and the effect of organic matter (OM) was not accounted for (Du et al., 2014). Recent studies have shown that OM may not affect PFAS removal (Sgroi et al., 2018a) or may positively

influence the PFAS adsorption (McCleaf et al., 2017). However, natural organic matter (NOM) and effluent organic matter (EfOM) often play a competitive role in the adsorption process (Appleman et al., 2013; Kothawala et al., 2017). Therefore, a critical review of the published data is needed to better understand the OM effect on long- and short-chain PFAS removal.

Furthermore, the regeneration of adsorbents exhausted by PFAS is not fully addressed (Woodard et al., 2017). Since PFAS breakthrough is fast, adsorbent regeneration is a very important and challenging task.

Previous published review papers deals with PFAS classification and origins (Buck et al., 2011; Xiao, 2017), their occurrence and fate in aquatic environments (Ahrens, 2011; Arvaniti and Stasinakis, 2015; Rahman et al., 2014) and the treatment technologies for long-chain PFAS removal (Appleman et al., 2014; Kucharzyk et al., 2017). A critical review concerning PFAS adsorption previously published is mainly concerned with PFOS and PFOA (Du et al., 2014) and it does not include recent scientific findings on OM effect as well as the performance and the regeneration of novel adsorbents. Recently, the removal of short-chain PFAS by different processes, including different adsorbents, has been critically reviewed by Ateia et al. (2019). However, such prior review papers concerning PFAS adsorption were not focused on the role of PFAS chain length, OM effect and adsorbents regeneration.

Therefore, the objective of this paper is to critically discuss data concerning PFAS adsorption with particular focus on: 1) recent published data about adsorption capacity of different materials for both long- and short-chain PFAS; 2) effect of OM on the PFAS adsorption; 3) role of adsorbent regeneration.

3. Adsorption of long chain PFAS

3.1. PFOA and PFOS

A number of studies have been carried out worldwide in order to investigate long-chain PFAS removal by adsorption on different materials. PFOA and PFOS are commonly regarded as the most representative PFAS, due to their persistence in the environment and occurrence in industrial applications. A prior review paper indicated that long-chain PFAS (i.e., PFOA and PFOS) have been mainly removed through hydrophobic interactions and adsorbents with amine groups generally have high adsorption capacity (Du et al., 2014).

The adsorption of long-chain PFAS on different adsorbents (commercially available or synthetized) obtained from batch adsorption tests is discussed in the following sections. Table 2 reports the adsorption capacity obtained from published data fitting the Langmuir model along with adsorbent material type and dosage, long-chain PFAS initial concentrations and experimental setups.

3.2. Activated carbon and biochar

Among commercial adsorbents, activated carbon (AC) has been widely investigated for PFOS and PFOA removal (Liang et al., 2011; Ochoa-Herrera and Sierra-Alvarez, 2008; Rattanaoudom et al., 2012). In detail, powdered activated carbon (PAC) had higher adsorption capacity than granular activated carbon (GAC) for both PFOA and PFOS (Chen et al., 2017; Yu et al., 2009).

Results about adsorption of PFOA on bamboo-derived activated carbon (BdAC) have shown that a long time (about 34 h) was required to reach adsorption equilibrium (Du et al., 2015). The comparison between BdAC and microporous AC revealed that the adsorption capacity of BdAC was higher than that of microporous AC (Du et al., 2015;

338 Wang et al., 2016). This evidence corroborates that microporous adsorbents are not
339 suitable for removing large molecules (i.e., long-chain PFSAs and PFCAs) and it is in
340 agreement with results from fixed-bed column tests, as detailed below (Appleman et al.,
341 2013; Du et al., 2014; McCleaf et al., 2017; Rattanaoudom et al., 2012; Zaggia et al.,
342 2016).

343 Chlorinated polyfluorinated ether sulfonate (F-53B) is a PFOS alternative compound.
344 Both F-53B and PFOS compounds have been detected at high concentrations in an
345 actual chrome plating WW (Du et al., 2016a). Electroplating wastewater treatment plant
346 (EWTP), employing reduction reaction (adding $Na_2S_2O_5$), precipitation (adding
347 $Ca(OH)_2$), and flocculation–sedimentation (adding anionic polyacrylamide, PAM), was
348 unable to effectively remove PFOS and F-53B. Hence, batch adsorption experiments
349 were performed and a commercial coconut shell based GAC (R-CAC), after an
350 activation process at low KOH/C ratio, was selected as adsorbent material for PFOS
351 and F-53B removal (Du et al., 2016a). F-53B is more hydrophobic than PFOS, due to
352 an ether unit in the molecular structure, and this led to a much higher adsorption
353 capacity of F-53B (two-fold higher than PFOS) onto R-CAC (Table 2). Single walled
354 carbon nanotubes (SWNT) are hollow cylindrical tubes, made of graphene layers and a
355 lattice of C atoms, and they have been investigated for PFOS and PFOA removal
356 (Wang et al., 2016). The comparison of microporous AC efficiency with SWNT, in
357 removing PFOA at the same concentration, revealed that microporous AC has a higher
358 adsorption capacity than SWNT. This difference may be linked to the higher surface
359 area of microporous AC than that of SWNT (Table 2). Moreover, adsorption capacities
360 of SWNT and AC for PFOS were 6 and 2 times higher, respectively, than that of PFOA,

probably due to the one more C-F unit of the PFOS molecule (Wang et al., 2016). In addition, SWNT exhibited higher adsorption capacity than multi walled carbon nanotubes (MWNT), consistent with their higher Brunauer, Emmett and Teller (BET) surface area (Chen et al., 2011; Li et al., 2011).

PFAS adsorption on biochar has also been investigated because of its cost-effectiveness and affinity with organic compounds (Guo et al., 2017; Inyang and Dickenson, 2017; X. Xiao et al., 2017).

Pinewood (PWC) and hardwood (HWC) biochars have been tested for PFOA removal and the adsorption capacity of the biochar was lower than that of AC (Table 2). Guo et al. (2017) have demonstrated that the adsorption capacity of corn-straw-derived biochar for PFOS removal increased with the increase of pyrolytic temperature, which is related to BET surface area of biochar (Table 2).

Reported data from fixed-bed column tests showed the ability of GAC to remove traces of PFAS (as both complex mixture or single solute) from water intended for human consumption (Appleman et al., 2014; Chularueangaksorn et al., 2014; McCleaf et al., 2017; Pramanik et al., 2017, 2015; Sgroi et al., 2018a; Zaggia et al., 2016). GAC (Filtrasorb 400, Calgon) column tested for PFOA removal has shown that the bed volumes were about 55,000 at 90% breakthrough point (Chularueangaksorn et al., 2014). The same GAC (Filtrasorb 400, Calgon) has been tested for long-chain PFCAs (i.e., PFOA, PFNA, PFDA, PFUnA, PFDoDA, PFTeDA) and PFSAs (i.e., PFHxS and PFOS) removal, and the observed removal efficiencies were in the range 65-80% (McCleaf et al., 2017). Information about the influence of GAC pore distribution on adsorption capacity of PFOS and PFOA were reported by Zaggia et al. (2016). Results

384 from continuous adsorption experiments have demonstrated the great efficiency of
385 bituminous AC, characterized by meso- and macropores, for PFOA and PFOS removal,
386 whose maximum adsorption capacity was 39.6 and 4.1 μg g^{-1}, respectively (Zaggia et
387 al., 2016). In fact, meso- and macro-porous adsorbent materials are more easily
388 accessed by long-chain PFAS resulting in higher adsorption capacity (Kothawala et al.,
389 2017; McCleaf et al., 2017; Zaggia et al., 2016). A high dosage of GAC (Filtrasorb 400,
390 Calgon) was tested in a pre-equilibrium batch study for the removal of a complex
391 mixture of long-chain PFSAs (PFHxS and PFOS) and PFCAs (PFOA, PFNA, PFDA,
392 PFUnDA, PFDoDA) from LW (Kothawala et al., 2017). Regardless of OM concentration,
393 long-chain PFAS removal was in the range of 50-90% (Kothawala et al., 2017).
394 However, these results were obtained from a pre-equilibrium study (contact time was 15
395 min) with a GAC dose (10 g L^{-1}) that is not typically employed at water treatment plants.

396 ### 3.3. Molecularly imprinted polymers

397 Several experimental works have explored the PFAS adsorption onto synthetically
398 modified polymers, which are adsorbents conveniently synthetized to have high affinity
399 and selectivity towards the target contaminants (Guo et al., 2018; Karoyo and Wilson,
400 2016; L. Xiao et al., 2017). The macromolecular imprinted materials (MIMs), containing
401 β-Cyclodextrin (β-CD) within a urethane framework, provide two types of binding sites.
402 One binding site is a β-CD inclusion site, the second is a non-inclusion (interstitial) site
403 of the cross-linker domains, where aggregates, micelles and other inclusion complexes
404 could be formed (Karoyo and Wilson, 2016). Formation of bilayer and multilayer
405 structures is the dominant adsorption process for both PFOA and PFOS in these
406 materials, as observed in several studies (Du et al., 2014; Gao et al., 2017; Karoyo and
407 Wilson, 2016). The modification of CD-based polymer adsorbents composition may

allow an increasing of PFOA removal (L. Xiao et al., 2017). Nevertheless, the removal efficiency of cross-linked polymer network, where β-CD substitutes decafluorobiphenyl (DFB-CDP), was comparable with that of biochar tested by Inyang and Dickenson (2017). Adsorption efficiency of non-imprinted carbon microspheres (NIP-CMs) for PFOS removal has been compared with a surface imprinted polymer (MIP-CMs) in which double functional monomers of methacryloyloxyethyl trimethyl ammonium chloride (DMC) and 2-(trifluoromethyl)acrylic acid (TFMA) have been synthetized on carbon microspheres (Guo et al., 2018). The adsorption capacity was higher for MIP-CMs than NIP-CMs (Table 2), due to the effect of molecularly imprinting technique in enhancing PFOS removal. The molecular imprinting technique has also been employed in order to prepare a novel adsorbent using chitosan crosslinked for PFOS removal and its adsorption capacity was higher than that observed for non-imprinted ones (Yu et al., 2008).

3.4. Anion-exchange resin

Several studies have indicated the suitability of the AE process for PFAS removal. Otherwise, PFAS removal efficiency varied greatly among AE resins, due to their properties, such as polymer matrix, functional group and porosity (Zaggia et al., 2016). It was demonstrated that large pores of macroporous resin allow a faster diffusion of PFOS than the gel one (Deng et al., 2010). This evidence is confirmed by comparing the adsorption capacity of IRA910 (polystyrene-DVB, macroporous-type) and IRA400 (styrene-DVB, gel-type) for PFOS removal (Maimaiti et al., 2018; Wang et al., 2016; Yu et al., 2009). Moreover, polymer matrixes led to different intraparticle diffusion and a polyacrylic resin has shown higher efficiency for PFOS removal than polystyrene one (Deng et al., 2010). IRA910 exhibited a good selectivity also for PFHxS as

demonstrated by Maimaiti et al. (2018). When IRA67 (polyacrylic-DVB, gel-type) has been employed, its adsorption capacity was higher than styrene type resins (Table 2). Gao et al. (2017) demonstrated the great applicability of polyacrylic resin for F-53B removal, since the adsorption capacity of IRA67 (about 2400 mg g^{-1}) was higher than that of R-CAC in batch experiments (Table 2).

As regards long-chain PFCAs, PFOA removal has been investigated on different kinds of strong AE resins (Du et al., 2015; Maimaiti et al., 2018; Wang et al., 2016; Yu et al., 2009). Based on Table 2, the highest adsorption capacity was obtained when IRA910 (polystyrene-DVB, macroporous-type resin) was employed (Maimaiti et al., 2018). The adsorption capacity of IRA67 was higher than that of BdAC, both adsorbents tested at the same PFOA initial concentration (Table 2). The efficiency of IRA67 may be ascribed to the amine groups on the resin surface, which involve the PFOA adsorption via AE mechanisms. Besides, the open pore structure of IRA67 also allowed a better diffusion of PFOA molecules. Moreover, as demonstrated by Zaggia et al. (2016), the selectivity of larger and more hydrophobic anions (i.e., PFOS and PFOA) increased with the increasing of alkyl chain length of the functional group of AE resins. Differences in terms of equilibrium exchange capacity of different type of resins are linked with the strength of hydrophobic interactions between resin functional groups and PFAS molecules. Considering hydrophobicity of resin, highly hydrophobic resins (such as A532E) favour PFOA and PFOS passage from hydrated state to adsorbed state as confirmed by the highest adsorption capacity values obtained on both batch and continuous-flow pilot scale experiments (Zaggia et al., 2016). The comparison between the performance of

AE resin and GAC for long-chain PFAS removal has also been carried out by employing the fixed-bed column tests.

Particularly, as demonstrated by Chularueangaksorn et al. (2014), PFA300 (AE resin, polystyrene crosslinked DVB) could treat a higher amount of water than GAC (Filtrasorb 400, Calgon) before the saturation (at a 90% breakthrough point, bed volumes were 119,880 and 55,080, respectively). A532E (polystyrene-DVB gel-type, bifunctional quaternary amine) exhibited the highest adsorption capacity for both PFOS and PFOA among several adsorbent materials tested (i.e., coconut based GAC, bituminous coal based GAC, mildly hydrophobic and non-hydrophobic resins) during continuous experiments (Zaggia et al., 2016). Removal efficiencies of AE resin (A600, polystyrene-DVB gel-type) for long-chain PFCAs (PFOA, PFNA, PFDA, PFUnA, PFDoDA, PFTeDA) and PFSAs (PFHxS and PFOS) were in the range 33-94% after 50,704 bed volumes (BVs), whereas removal efficiencies of GAC (Filtrasorb 400, Calgon) column were in the range 28-94% after 49,523 BVs (McCleaf et al., 2017).

3.5. Synthetized materials

With the purpose of identifying the best suitable adsorbent for PFAS removal, it is currently practice to synthesize new materials with properties and structures easy to control and modify. To date, new adsorbents with higher selectivity and specificity designed towards PFAS removal are also becoming commercially available for water treatment applications. For instance, a porous aromatic framework constructed from benzene rings (PAF-45) was employed for PFOS removal (Luo et al., 2016). Despite the remarkable adsorption capacity (Table 2), PAF-45 feasibility was influenced by pH solution and ionic strength since the adsorption capacity was higher at acidic pH values (i.e., pH ~ 3). Moreover, the adsorption isotherm experiments have been carried out at

PFOS concentrations in the range of 50-200 mg L^{-1} (Luo et al., 2016), which are much higher than the PFAS concentrations typically detected in the water environment (Rahman et al., 2014).

Covalent triazine-based framework (CTF) has been investigated for removing different long-chain compounds (PFOA, PFHxS and PFOS), due to its large surface area and rigid pore structure (Wang et al., 2016). Among the three long-chain PFAS tested, Wang et al. (2016) have demonstrated that the adsorption capacity of CTF was highest for PFOS (Table 2). The electrostatic interaction between PFAS anion head and triazine groups of CTF (positively charged) represents the main driving force for PFAS adsorption on CTF. Based on electrostatic interactions, which are the main adsorption mechanism of short-chain PFAS, CTF exhibited a good adsorption capacity for PFBS and PFBA removal, as it will be discussed below.

Boron nitride, characterized by lightness structure and thermal stability, has been synthesized as porous hexagonal boron nitride nanosheets (h-BNs) for PFOS and PFDA removal (Feng et al., 2016). The efficiency of this adsorbent material has been demonstrated to be linked with chain length and functional group of PFAS, since PFDA was more favourable adsorbed than PFOS (adsorption capacity of 0.16 mg m^{-2} and 0.04 mg m^{-2}, respectively). Among novel adsorbent materials investigated, magnetic-nanoparticles attached into fluorographene (2-MNPs@FG, mass ratio of MNPs and FG is 3:5) exhibited the highest adsorption capacity for PFOS instead of PFOA (Table 2). However, adsorbent dosage was not coherent with that really employed in full-scale treatment plants (Wang et al., 2018).

Quaternized cotton and aminated rice husk (ARH) both prepared with atom transfer radical polymerization (ATRP) technique were tested for PFOS and PFOA removal (Deng et al., 2013, 2012). Results have demonstrated that quaternized cotton had higher adsorption capacity than ARH for both PFOS and PFOA (Table 2).

Polyacrylonitrile fiber (PANF)-derived activated carbon fibers (PACFs) showed a remarkable adsorption capacity for PFOS and PFOA (Chen et al., 2017). The adsorption affinity could be ascribed to its high specific surface area and micro- and mesoporous structure which allowed the establishment of multilayer adsorption (formation of hemi-micelles and micelles). The latter was also the main adsorption mechanism on crosslinked chitosan beads employed for PFOS removal, as demonstrated by Zhang et al. (2011).

Poly(ethylenimine)-functionalized cellulose microcrystals (PEI-f-CMC) have been tested for removing long-chain PFAS at environmentally relevant concentration level (Ateia et al., 2018). Long-chain PFAS removal percentage was in the range of 80-98%. Despite its low surface area, PEI-f-CMC exhibited a good adsorption affinity both in DI and in the presence of co-existing OM, as discussed in section 5.

The main drawback of those synthetized materials is the application at full-scale treatment plants because their production is not industrialized and, probably, they are not commercially available, unlike AC and AE resins. Economic assessment for new synthetized materials is needed.

3.6. Nanoparticles materials

The adsorption of PFAS into nanoparticles (NPs) has recently been investigated due to their co-existing in aquatic environments (i.e., marine debris plastic) or their high surface area and reactivity (i.e., iron oxides). As demonstrated by Lu et al. (2016), nano-oxides

such as titania (TiO_2), iron oxides (Fe_2O_3), alumina (Al_2O_3) and silica (SiO_2) have the ability to sorb PFOS. Among the different nano-oxides tested, Al_2O_3 showed the highest PFOS adsorption capacity (1.1 μg m^{-2}), whereas SiO_2 exhibited the lower adsorption capacity (0.1 μg m^{-2}). This difference in terms of PFOS removal should be ascribed to the different hydroxyl groups and surface area. Furthermore, the main adsorption mechanism of PFOS on nano-oxides was not only electrostatic interaction, but also the formation of hydrogen bounds between the PFOS sulfonic terminal group and nano-oxides surface (Lu et al., 2016).

Magnetite nanoparticles (Fe_3O_4 NP) were used as the substrate of a novel magnetic nanocomposite (Fe_3O_4@SiO_2- NH_2&F_{13}), in which silica membrane functionalized with amino group and octyl-perfluorinated chain was synthesized on the Fe_3O_4 NP surface (Zhou et al., 2016). Based on kinetic data, the predominant adsorption mechanism between the magnetic adsorbent and PFAS tested was chemisorption, which includes both electrostatic and F-F interaction (Zhou et al., 2016). In detail, the selective F-F interaction between octyl-perfluorinated chain on the magnetic composite surface and perfluoroalkyl dipole shell in PFAS molecule was enhanced by electrostatic attraction of -NH_2 and the anionic -COOH or -SO_3H of PFCAs and PFSAs molecules, respectively. Due to size exclusion effect, PFCAs were better adsorbed than PFSAs on Fe_3O_4@SiO_2-NH_2&F_{13}. Considering perfluoroalkyl chain length, PFUnDA exhibited the highest adsorption capacity onto Fe_3O_4@SiO_2- NH_2&F_{13}, due to the formation of aggregate structure between long-chain PFAS which could stick together and, consequently, the amount of PFAS adsorbed increased (Zhou et al., 2016).

A recent experimental work investigated the capability of microplastics (MPLs) to sorb a complex mixture of PFAS from RW (Ebro river) and seawater (SeaW), simulating realistic environmental conditions (Llorca et al., 2018). High-density polyethylene (HDPE), polystyrene (PS) and poly-styrene carboxylic acid (PS-COOH) were selected due to their wide occurrence as marine debris plastic. Results of batch adsorption experiments showed low removal percentages (< 27%) of long-chain PFAS in RW after 7 days (with few exceptions of PFTrA and PFTeA whose percentages were between 65% and 70%). Moreover, MPLs efficiency in SeaW was affected by water chemistry such as salinity and OM concentration. This point will be deeply explained later (see section 5). Overall, carboxylated compounds with more than 11 C atoms were the most removed (Llorca et al., 2018). In detail, HDPE exhibited the worst adsorption capacity due to its granular shape, which limited the intraparticle diffusion (Llorca et al., 2018). In RW, PFOA, PFNA, PFHxS and PFOS did not present any adsorption on both HDPE and PS-COOH throughout the experiment period. On the contrary, affinity between carboxylated compounds with less than 10 C atoms and HDPE was higher in SeaW.

Adsorption rates of PFCAs on PS-COOH in RW increased with the increasing of chain length. Comparing PFCAs to PFSAs, with the same chain length, the carboxylated compounds were less removed (Llorca et al., 2018). Whereas, in SeaW, the presence of carboxylic group in the PS-COOH surface implicated an increase of adsorption rates of carboxylated compounds. Adsorption kinetics were influenced by adsorbents size, therefore PS exhibited faster kinetic than HDPE, since it had the smallest particles (Llorca et al., 2018).

4. Adsorption of short chain PFAS

4.1. Challenges in short chain PFAS adsorption

Short-chain PFAS and their precursors are as persistent as those long-chained. Therefore, although they show less bioaccumulation potential, their environmental occurrence is of concern (Ateia et al., 2019; Brendel et al., 2018; Zhao et al., 2016). While long-chain PFAS are binding with particles present in solution, those short-chain are mainly in the dissolved phase resulting in long-range transport in aquatic environments (Ahrens, 2011). Therefore, short-chain PFAS have higher mobility in water bodies than long-chain compounds. Specifically, short-chain compounds could significantly affect drinking water supplies, increasing the human exposure to PFAS compounds. Considering the properties of short-chain PFAS (Table 1), it is expected that the large-scale remediation treatments, currently suitable for long-chain PFAS, are ineffective for short-chain PFAS (Ateia et al., 2019; Brendel et al., 2018). This evidence is consistent with data from full-scale drinking water treatment plants (Arvaniti and Stasinakis, 2015; Rahman et al., 2014). Moreover, it is widely reported that carbon-chain length influences adsorption capacities of PFAS onto various materials, since adsorption rate seems to increase with the increase of molecular size (Appleman et al., 2014).

Data collected from full-scale treatment plants (drinking and wastewater facilities) suggested that the removal of short-chain compounds is still a challenge task, due to their early and faster breakthrough (Arvaniti and Stasinakis, 2015; McCleaf et al., 2017; Zaggia et al., 2016). To date, a restricted number of published data have addressed short-chain PFAS adsorption by using different materials, because most of the experimental works have focused on the removal of long-chain PFAS (i.e., PFOA and

PFOS). Adsorption capacities obtained by fitting the Langmuir model along with type and dosage of adsorbent materials, initial concentration of short-chain PFAS and experimental setup are reported in Table 3. Comparisons between several adsorbent materials tested for short-chain PFAS are reviewed based on both batch experiment studies (Table 3) and fixed-bed column tests.

The adsorption capacity of materials tested for PFBA removal observed during batch tests (Table 3) follows the order: microporous AC < CTF < IRA910 (strong AE resin). However, results obtained by continuous experiments have demonstrated that the adsorption capacity of meso-porous GAC (meso-porous bituminous coal-derived AC) was higher than A532E (strong AE resin) (4.3 and 3.3 μg g^{-1}, respectively) (Zaggia et al., 2016). In the following sections the removal of short chain PFAS by adsorption is discussed based on the type of adsorbent.

4.2. Activated carbon, biochar and other adsorbents

The performance of BdAC and coal-based AC (microporous type), used for removing PFHxA, has been compared. The adsorption capacity of BdAC was 13 times lower than microporous AC probably due to its low BET surface area and the presence of OM in the solution tested (Du et al., 2015; Wang et al., 2016). The adsorption capacities of HWC and PWC biochars for PFBA and PFOA removal were investigated by Inyang and Dickenson (2017). Results from adsorption kinetic tests showed that the amount of PFBA adsorbed on both HWC and PWC was 3-4 times lower than that of PFOA. This evidence suggests the incapability of biochar for short-chain PFAS removal and it may prove the competition between long- and short-chain PFAS for the adsorption sites and/or competition with OM (Inyang and Dickenson, 2017).

615 Short-chain PFAS adsorption on GAC and PAC has also been investigated by using
616 batch test (Hansen et al., 2010). Tests have been carried out at real concentrations of
617 short-chain PFAS (range about 73 – 320 ng L^{-1}) and using an adsorbent dose
618 comparable to that used in real water treatment plants (range about 25 – 125 mg L^{-1}).
619 Results have demonstrated that PAC has higher adsorption capacity than GAC (more
620 than twice), due to the shorter internal diffusion distances and its higher BET surface
621 area (Hansen et al., 2010).
622 MWCNTs functionalized in different ways (MWCNTs-PRI, MWCNTs-COOH, MWCNTs-
623 OH) were tested for PFBS removal (Deng et al., 2015a). Removal percentage of PFBS
624 on MWCNTs was about 30% in DI water, whereas when humic acids (HA) and phenol
625 co-existed in the solution, this percentage was lower than 20% (Deng et al., 2015a).
626 Moreover, due to the weak hydrophobicity of PFBS, its percentage removal was lower
627 than that of long-chain compounds (Deng et al., 2015a). Results of adsorption isotherm
628 of PFOS and PFBS on boehmite showed that PFOS was better removed than PFBS,
629 since the effect of surface aggregation enhanced long-chain PFAS removal (Wang et
630 al., 2015).
631 Among fixed-bed column experiments carried out in order to assert the short-chain
632 PFAS removal, McCleaf et al. (2017) reported faster breakthrough and lower removal
633 percentage of short-chain PFCAs on GAC column (F400, Calgon) than long-chain ones.
634 The removal efficiencies of the short-chain PFCAs tested (i.e., PFBA, PFPeA, PFHxA
635 and PFHpA) were lower than 19% on GAC column after 49,523 BVs. Whereas, the
636 removal efficiency of PFBS (short-chained PFSAs tested) was ~10%. Those results
637 suggest that short-chain PFAS removal depends mainly on the availability of active

638 sites, since they do not bind with other particles and, consequently, the formation of
639 aggregates does not occur (McCleaf et al., 2017; Zaggia et al., 2016). Moreover,
640 desorption of short-chain PFAS has been also hypothesized, due to the competition of
641 long-chain PFAS and/or OM. Similar fast breakthrough of short-chain PFAS has also
642 been observed in rapid small-scale column tests (RSSCT) carried out on different types
643 of GAC columns (Appleman et al., 2013). Among the three activated carbons tested,
644 F300 (microporous bituminous coal-derived) exhibited the lowest efficiency for the
645 short-chain PFCAs tested (i.e., PFBA, PFPeA and PFHxA), due to its pores distribution
646 (mainly microporous type) and BET surface area. Others GAC tested, coconut based
647 GAC (AquaCarb 1240) and bituminous coal based ones (F600), performed better for
648 the removal of selected short-chain PFAS (Appleman et al., 2013).
649 PFBA uptake on different types of biochar was influenced by BET surface area. Indeed,
650 the highest percentage removal has been found on the hardwood sawdust pellets
651 gasified at 900 °C (HWC), which had the highest BET surface area among the different
652 biochars tested (Inyang and Dickenson, 2017). However, results obtained from batch
653 adsorption kinetic tests have demonstrated that GAC removed PFBA better than HWC
654 (Inyang and Dickenson, 2017).
655 Short-chain PFAS adsorption on microplastics (HDPE, PS and PS-COOH) has recently
656 been investigated in simulated realistic environmental conditions (Llorca et al., 2018).
657 Due to the increase in ionic strength, short-chain carboxylates compounds have been
658 better removed by PS-COOH in SeaW than in RW. Whereas, short chain PFAS were
659 almost not adsorbed onto PS and HDPE (Llorca et al., 2018).

Removal of PFBS (short-chain PFSAs) has been investigated at batch mode by means of AC (i.e., microporous AC and Calgon F400) and CTF (Ochoa-Herrera and Sierra-Alvarez, 2008; Wang et al., 2016). The difference of adsorption capacity between CTF and AC may be related to their different structure and, consequently, adsorption mechanisms established, since the electrostatic interactions between PFAS anion head and triazine groups of CTF involved short-chain PFAS adsorption on CTF (Wang et al., 2016). However, CTF exhibited a lower affinity with PFBA than ARH (Table 3). Adsorption capacity of ARH was 4 times higher than CTF (Deng et al., 2013; Wang et al., 2016).

A novel adsorbent poly(ethylenimine)-functionalized cellulose microcrystal (PEI-f-CMC) has been synthetized and its efficiency for short-chain removal has been evaluated at environmental relevant concentration levels (Ateia et al., 2018). Results have demonstrated that short-chain with sulfonate terminal group were removed better than short-chain PFCAs, in agreement with previous experimental studies (McCleaf et al., 2017; Rahman et al., 2014).

4.3. Anion-exchange

The removal efficiency of three PFCAs owning different chain lengths, including PFHxA (with 6 C atoms), PFHpA (with 7 C atoms) and PFOA (with 8 C atoms) from industrial WW (perfluorooctanesulfonyl fluoride washing wastewater, PFSOF WWW) by AE resin has been evaluated during batch experiments conducted by Du et al. (2015). Results demonstrated that adsorption sites on IRA67 were occupied by PFOA molecules prior to the others PFCAs and, therefore, the adsorption rates of short-chain were lower. Consequently, short-chain PFCAs reached the equilibrium very fast (Du et al., 2015). Moreover, comparing the efficiency of two different anion-exchange resins (i.e., IRA910

and IRA67) for removing the same compound (PFHxA), IRA910 (polystyrene-DVB macroporous-type) exhibited higher adsorption capacity than IRA67 (polyacrylic-DVB gel-type) (Du et al., 2015; Maimaiti et al., 2018). This difference in adsorption capacity for PFHxA may be linked to the resin properties, such as polymer matrix and porosity, and/or to the effect of OM present in the solution. In fact, IRA910 was tested in DI water, whereas IRA67 was employed for PFHxA removal from PFSOF WWW (Du et al., 2015; Maimaiti et al., 2018).

Moreover, when tested for the same actual WW, IRA67 had higher affinity with PFHpA than BdAC, as demonstrated by the adsorption capacity, which was 3 times higher than that of BdAC (Du et al., 2015). Furthermore, amine groups on adsorbent surface improved the short-chain PFAS removal, due to the establishment of electrostatic interactions, which are the main driving force during short-chain adsorption (Deng et al., 2013; Du et al., 2014; Zhang et al., 2011). Results provided by fixed-bed column tests demonstrated that the adsorption capacity of A532E (strong AE resin) was almost equal to that of GAC (meso-porous bituminous-coal derived AC), when tested for PFBS removal (4.7 μg g^{-1} and 4.1 μg g^{-1}, respectively) (Zaggia et al., 2016).

Results from fixed-bed column experiments carried out by McCleaf et al. (2017) have shown fast breakthrough and low removal percentage for short-chain PFCAs on AE resin (A600, polystyrene-DVB gel-type). The removal efficiencies of short-chained PFCAs tested were ~11% on A600 column after 50,704 BVs. The same anion-exchange resin better removed PFBS (short-chain PFSAs tested) than other short-chain compounds, and the removal efficiency of PFBS was ~55% (McCleaf et al., 2017).

Results from a pre-equilibrium study carried out by Kothawala et al. (2017) demonstrated that fresh adsorbent materials (i.e., AE resin, Purolite A600, and GAC, Filtrasorb 400) could remove short-chain PFAS from water solutions. Nevertheless, anion-exchange showed the highest percent of removal. In detail, removal percentages of short-chain PFAS (PFBA, PFPeA, PFHxA, PFHpA, PFBS) were about 90% and 50% on A600 and Filtrasorb 400, respectively. However, those results have been obtained from a pre-equilibrium study (contact time was equal to 15 min) with a high dosage of adsorbent materials (Kothawala et al., 2017).

Analysis of transmission electron microscopy (TEM) carried out on AE resins allowed a deep understanding of the predominant adsorption mechanism involved during short-chain PFAS removal (Zaggia et al., 2016). Indeed, TEM images showed that the weak hydrophobic interactions between PFBA (or PFBS) and resin surface did not allow the formation of aggregates and, consequently, AE of single molecules was the main mechanism for short-chain removal.

Overall, AE resins exhibit a remarkable adsorption capacity for both long- and short-chain PFAS. Nevertheless, the possible release of disinfection by-products (DBP) such as N-Nitrosodimethylamine (NDMA) may represent the main drawback for their full-

scale application (Sgroi et al., 2018b). Particularly, the amount of NDMA and their precursors released upon usage depends on the resin functional group (such as amine groups) and operational conditions (such as regeneration activities and flow interruptions).

4.4. Comparison between long- and short-chain PFAS adsorption

In order to provide a deeper analysis on the long- and short-chain PFAS removal by adsorption, data from Table 2 and Table 3 have been elaborated to build a box-and-whiskers plot (Figure 1) that allows the comparison between the removals of long- and short-chain PFAS by different adsorbents (classified as activated carbon, resin, and synthetized materials). Figure 1 shows that the adsorption capacity of a wide range of adsorbents is lower for short-chain PFAS compared to that observed for long-chain PFAS. This result emphasizes that the removal of short-chain PFAS by adsorption is very challenging and it will need more research in the future. A comparison in adsorption capacity of the different adsorbents employed have shown that resins are more effective than activated carbons for both long- and short-chain PFAS removal. Activated carbon exhibited the lowest adsorption capacity. A significant variation in adsorption capacity of synthetized materials used for long-chain removal was observed. Such variation ranged from the lowest to the highest adsorption capacity observed for long-chain PFAS removal. However, the latter best results were often obtained at acid pH. For instance, the best adsorption capacity (5847 mg g^{-1}) was found by using the PAF-45 adsorbent at pH 3. Therefore, the real operating conditions may affect the removal efficiency. For instance, the effect OM may significantly influence the performance of adsorbents, as discussed in the next section.

5. Effect of organic matter (OM) on PFAS adsorption

5.1. PFAS adsorption in presence of OM

OM is ubiquitous in the aquatic environment and it can be distinguished between NOM, regarded as OM naturally present in surface water, and EfOM, the OM released from WWTPs (Shon et al., 2006).

OM could affect adsorption efficiency of adsorbent materials due to binding and adsorption interactions with PFAS, including long- and short-chain compounds. As illustrated by Du et al. (2014b), NOM could interact with PFAS via electrostatic and/or hydrophobic interactions. Firstly, OM is mostly constituted of anionic species and, after adsorbing on materials, it can lead to repulsive electrostatic interactions. Meanwhile, NOM can also lead to PFAS adsorption via hydrophobic interaction between perfluoroalkyl tail and NOM adsorbed on the adsorbent surfaces. To date, it is not well understood how these effects co-exist and which is predominant.

Most of undertaken experimental works investigated adsorption properties of PFAS on different adsorbent materials in DI (Deng et al., 2012; Guo et al., 2018; Maimaiti et al., 2018; Yu et al., 2009). Many researches have selected fulvic and humic acids (FA and HA) as the model DOM in order to evaluate the impact of DOM on PFAS adsorption (Deng et al., 2015a; Du et al., 2016b; Maimaiti et al., 2018; Pramanik et al., 2015; F. Wang et al., 2015; L. Xiao et al., 2017). Actually, NOM consists of a wide range of organic compounds, such as hydrophilic acids, proteins, carboxylic and amino acids in addition to the already mentioned HA and FA. When using a synthetic solution of OM during experimental studies, some interactions between PFAS and water matrix have not been described in detail. Table 4 reports the main experimental works published related to the adsorption of PFAS (both long- and short-chain compounds) on different

771 adsorbent materials in the presence of OM. However, some of those studies lacked a
772 detailed discussion on the effect of OM on PFAS adsorption.
773 Most of these experimental studies (Appleman et al., 2013; Du et al., 2016b, 2016a; Y.
774 Wang et al., 2015; L. Xiao et al., 2017) have investigated the effect of OM on PFAS
775 adsorption through comparison between synthetic OM solution and OM free solution
776 (Table 4). Only few experimental works compared the effect of different DOM sources
777 on PFAS adsorption and tested water had different dissolved organic carbon (DOC)
778 concentrations (Ateia et al., 2018; Inyang and Dickenson, 2017; Kothawala et al., 2017;
779 Sgroi et al., 2018a; Wang et al., 2018) . Furthermore, the simultaneous effect of ionic
780 strength and OM on the PFAS adsorption is very complex. For instance, it was
781 demonstrated that the presence of monovalent and divalent cations increases PFAS
782 adsorption on different materials, i.e. sediments (Higgins and Luthy, 2006), activated
783 carbon (Du et al., 2015), synthesized material (PAF-45) (Luo et al. 2016), resin (Du et
784 al., 2015) and kaolite (Xiao et al., 2011). Particularly, the adsorption of short-chain
785 PFAS (i.e., PFHxA and PFBA) on kaolinite was more thermodynamically favorable at a
786 higher Na^+ concentration due to the compression of the electrical double layer and
787 ensuing reduced electrostatic repulsion between PFAS and kaolite surface (Xiao et al.,
788 2011). In addition, divalent cations (such as Ca^{2+} and Mg^{2+}) could also improve PFAS
789 removal by divalent cation-bridging effect (Du et al., 2015, 2014). On the contrary, the
790 presence of inorganic anion negatively affects the adsorption of PFAS due to the
791 competition for adsorption sites (Deng et al., 2010). Whereas, it was observed that the
792 presence of ionic OM (i.e., HA, SDS, FA) compete with both long- (F. Wang et al., 2015;
793 Zhao et al., 2011) and short-chain PFAS (Maimaiti et al., 2018; Zhao et al., 2011).

794 Specifically, such effect seems more relevant for short-chain PFAS due to the
795 competition for active sites (Maimaiti et al., 2018; McCleaf et al., 2017; Zhao et al.,
796 2011). On the other hand, hydrophobic DOM was found to improve the PFAS retention
797 in GAC adsorption, while hydrophilic DOM seems do not affect significantly PFAS
798 adsorption in both GAC and AE adsorption experiments (Kothawala et al., 2017). The
799 positive impact of DOM on the adsorption of long-chain PFAS has been ascribed to the
800 formation of PFAS aggregate or DOM-PFAS complexes (Kothawala et al., 2017;
801 McCleaf et al., 2017) but such bonds have been rarely demonstrated. Consequently,
802 the impact of DOM and ionic strength on the PFAS adsorption need more investigation.
803 A systematic review concerning the effect of OM on PFAS adsorption for different
804 classes of adsorbents is reported in the following sections.

805 ## 5.2. Activated carbon

806 Among adsorbent materials, AC has proven to be effective for PFAS removal and its
807 efficiency in presence of OM has been investigated both in batch and column
808 experiments (Table 4). Contrasting trends have been observed in experimental studies
809 because of the influence of co-existing OM. Indeed, the performance of PFAS
810 adsorption onto AC was found negatively impacted, enhanced or not influenced by the
811 presence of OM. The main interactions that could be established between OM
812 molecules and PFAS (both long- and short-chain) during adsorption on GAC column are
813 illustrated in Figure 2. In detail, hydrophobic interactions mainly concern long-chained
814 C-F molecules, while short-chain PFAS interact with OM molecules through pore
815 blockage and electrostatic repulsions.
816 In many cases, activated carbon performance was negatively influenced by co-existing
817 OM and its efficiency decreased with the increase of DOC concentrations (Du et al.,

2016a, 2015; Hansen et al., 2010; Kothawala et al., 2017; Pramanik et al., 2017, 2015; Y. Wang et al., 2015; Yu et al., 2012; Zhao et al., 2011). On the contrary, adsorption capacity on GAC did not significantly decrease in the presence of GW NOM probably due to the high concentration of PFAS tested (50 mg L^{-1}) and to the effect of ionic strength (Zhao et al., 2011). Results from the previously mentioned study demonstrated that PFBA removal was affected by OM since the results from adsorption equilibrium suggested a reduction of 40% (Zhao et al., 2011). Results from adsorption kinetic experiments provided by Yu et al. (2012) suggested that adsorption equilibrium for PFOA and PFOS on PAC was reached at 4 h and 24 h in the absence and in the presence of EfOM, respectively (Yu et al., 2012). The competition between PFAS and DOM for AC adsorption sites has also been investigated in RSSCTs (Appleman et al., 2013; McCleaf et al., 2017; Pramanik et al., 2017, 2015; Sgroi et al., 2018a). Results obtained from the latter mentioned experimental works are in disagreement about the effect of OM. This discrepancy may be related to the different experimental setups, such as PFAS initial concentration, source and concentration of DOM, empty bed contact time (EBCT), and to the kind of AC tested. As suggested by Pramanik et al (2015), when DOC concentration increased from 5 to 25 mg L^{-1} the removal efficiency of PFOA and PFOS on PAC decreased by 50% and 35%, respectively. On the contrary, the performance of bituminous coal-based GAC was less influenced by variation of DOC concentration (Pramanik et al., 2015). Similar results have asserted that proteins resulted in a low retention of PFOA and PFOS through hydrophobic and electrostatic interactions (Pramanik et al., 2017). Moreover, breakthrough > 20% has been reached at 125,000 BVs during DOM-free experiments, and at ~ 11,000 BVs when DOC

841 concentration was equal to 1.7 mg L^{-1}. This observation highlights that faster
842 breakthrough of PFAS takes place during RSSCT experiments in presence of DOM
843 (Appleman et al., 2013). Nevertheless, Sgroi et al. (2018a) found that breakthrough
844 curves of some long-chain PFAS (i.e., PFOS, PFOA and PFDA) were similar in column
845 beds packed tests by using Norit Darco 12x40. In those experiments, waters with
846 different DOM concentrations and compositions fed the packed columns (Table 4). The
847 observed behaviour for the investigated long-chain compounds may be ascribed to the
848 hydrophobic interactions occurring between long-chain PFAS and GAC. Indeed,
849 hydrophobic interactions are the main adsorption mechanisms for long-chain PFAS, and
850 the hydrophobic interactions may be only slightly influenced by OM presence.
851 Results of pre-equilibrium study by Kothawala et al. (2017) are in contrast with other
852 findings (Du et al., 2016a; Wang et al., 2016; Yu et al., 2012; Zhao et al., 2011), since
853 the increase in DOC concentration seems to enhance long-chain PFAS removal due to
854 the formation of DOM-PFAS complex and, consequently, their co-adsorption. In detail,
855 removal efficiency of PFAS with a fluorocarbon-chain length of 8 C atoms increased by
856 50% when DOC concentration of a hydrophobic DOM passed from 0 to 8 mg L^{-1} using
857 GAC (Kothawala et al., 2017). It should be highlighted that these results were obtained
858 in pre-equilibrium conditions (contact time about 15 min), at PFAS initial concentration
859 of about 2.5 µg L^{-1} and at batch dose of GAC of about 10 g L^{-1}, which is much higher
860 than doses typically used in full-scale treatment plants (Ziska et al., 2016). Performance
861 of BdAC for PFCAs removal from PFSOF WWW has been investigated in the presence
862 of high total organic carbon (TOC) concentration. Co-existing OM competed with
863 PFCAs for adsorption sites on the BdAC (Du et al., 2015). The same achievement was

obtained using R-CAC for PFOS and its alternative compound, F-53B, removal from electrochemical WWTP effluent (Du et al., 2016a). The high concentration of TOC (78.3 mg L^{-1}) was linked to the high amount of hydrocarbon surfactants which were unfavourable for the adsorption of PFOS and F-53B on R-CAC, since adsorption sites were manly occupied by co-existing organic compounds (Table 4). Depending on OM concentration and source, dose and kind of AC employed (powdered or granular, and its porosity), and PFAS tested (long- or short-chain), the effect of OM is different, due to adsorption mechanisms established. The presence of OM can lead to the enhancement of PFAS adsorption through the formation of agglomerations between long-chain PFAS and OM. Otherwise, OM can negatively influence the adsorption efficiency, due to the reducing of accessible binding sites and pore spaces (i.e., pore blockage) (Figure 2).

5.3. Anion-exchange resin

Main interactions occurring between OM and PFAS molecules during AE process are reported in Figure 3. As previously asserted about the influence of OM on AC performance, the effect of co-existing OM on AE resins for PFAS removal depends on several factors, including OM composition and concentration, kind of resin and PFAS concentration tested.

To date, the competition between OM and PFAS on AE resins is not fully understood. This evidence is confirmed by several experimental studies carried out both on batch and column setups (Du et al., 2015; Kothawala et al., 2017; Maimaiti et al., 2018; McCleaf et al., 2017; Wang et al., 2016; Zaggia et al., 2016). Organic compounds, such as HA, tri-chloroethylene (TCE), methylbenzene (MB) and sodium dodecyl sulphate (SDS), have been selected to evaluate their effect on PFHxS removal on AE resin (i.e., IRA910, a macroporous polystyrene resin with a dimethyl ethanol ammonium functional

888 group) during batch experiments (Maimaiti et al., 2018). Results suggested that PFHxS
889 retention on IRA910 was not affected by non-ionic co-existing organic compounds (i.e.,
890 MB and TCE), regardless of their concentration in the solution. Whereas, IRA910
891 efficiency decreased with the increasing of HA and SDS concentrations, due to the
892 competition for adsorption sites. A slight effect on PFAS retention has been highlighted
893 under pre-equilibrium condition since AE resin (A600, polystyrene-DVB gel-type with
894 quaternary ammonium functional group) performance was independent from DOM
895 concentration and source (Kothawala et al., 2017). In detail, PFAS removal has been
896 reduced by 10% at the highest DOM concentration tested. This result is consistent with
897 data reported by previous experimental works which have demonstrated that OM
898 weakly interferes with PFAS removal during AE process (Du et al., 2015; Wang et al.,
899 2016). Resins gel-type polymer matrixes, such as IRA400 and IRA67, showed a
900 remarkable affinity with PFAS (both long- and short-chain), which was independent of
901 OM present. In an opposed way, the performance of macroporous resins (i.e., IRA910)
902 could be affected by background DOM levels.

903 ### 5.4. Other adsorbents (biochar, multi-walled carbon nanotubes,
904 mineral materials, nanoparticles)

905 Effect of co-existing HA on boehmite surface was investigated during PFOS and PFBS
906 batch adsorption experiments (F. Wang et al., 2015). Due to the electrostatic
907 interactions between PFAS and boehmite, strong competition between PFOS (or PFBS)
908 and HA occurred. Electrostatic repulsions increased with the increasing of HA
909 accumulation on boehmite surface (F. Wang et al., 2015). The competition between
910 PFAS and synthetic OM (HA, phenol, 1-naphthol and benzoic acids) has also been
911 investigated on MWCNTs (Deng et al., 2015a). The pronounced influence on PFOS

912 removal was provided by HA, whereas phenol had a lesser influence. Moreover, PFBS
913 removal was the worst in the presence of HA or phenol (Deng et al., 2015a).
914 As demonstrated by Inyang and Dickenson (2017), HWC and PWC biochar
915 performances were affected by OM, since adsorption capacities decreased with the
916 increase of DOC concentration. In particular, OM molecules could lead to pore blockage
917 and may occupy high-energy pore sites. The adsorption capacities were about 41.3 and
918 27.7 mg g^{-1} when LW (DOC = 2 mg L^{-1}) and tertiary treated WW effluent (DOC = 4.9 mg
919 L^{-1}) were tested, respectively (Inyang and Dickenson, 2017). Results from pilot-scale
920 tests have demonstrated that the breakthrough of some PFAS (i.e., PFPeA, PFHxA,
921 PFOA and PFOS) was faster on biochar HWC filter than on GAC column, since OM
922 adsorbed on biochar surface caused changes on biochar surface charge.
923 Consequently, the electrostatic repulsions between PFAS and biochar surface
924 increased. Adsorption kinetic tests were performed for both PFBA and PFOS, and the
925 observed slow kinetics could have been caused by pre-loaded OM on biochar (Inyang
926 and Dickenson, 2017).
927 The efficiency of novel magnetic adsorbent,2-MNPs@FG, has been investigated for
928 PFOA and PFOS removal from different water matrixes (Wang et al., 2018). Its
929 performance was independent of OM content also at the highest DOC concentration
930 tested (1.7 mg L^{-1}). Indeed, the removal efficiencies were always found around 99% for
931 both PFOA and PFOS in all performed experiments. However, it should be noted that
932 those efficiencies have probably been obtained because of a high dosage of adsorbent
933 employed (400 mg L^{-1}). The competition between NOM (both SeaW and RW) and PFAS
934 (both long- and short-chain compounds) has also been investigated during PFAS

adsorption onto HDPE, PS and PS-COOH particles (Llorca et al., 2018). Results asserted that aromatic rings of PS contrasted NOM competition and, consequently, they favoured PFAS adsorption. By contrast, NOM influenced PFAS adsorption on HDPE and its effect was higher in SeaW than in RW (Llorca et al., 2018). Sun et al. (2018) investigated the effect of co-existing organic compounds on GAC biofilter. They reported that more active sites were available for PFAS adsorption in the pre-ozonated regenerated GAC biofilter, due to the oxidation of competitive DOM (Sun et al., 2018).

Recently, the performance of new synthetized adsorbent (PEI-f-CMC) for PFAS removal (both long- and short-chain) was evaluated using three different NOM solutions (Ateia et al., 2018). Firstly, experiments were carried out in LW (Hartwell Lake, South Carolina) and PFAS removal efficiency has been compared with that resulted from DOC free solution. PFOA and PFOS removal efficiency was almost equal in both LW and DI. PFAS with longer chain than PFOA and PFOS (C_{12} – C_{13} PFCAs, C_9 – C_{10} PFSAs) were removed better from LW than from DI using PEI-f-CMC. This result can be explained by the co-removal of long-chain PFAS aggregated with OM (Du et al., 2014; McCleaf et al., 2017). By contrast, short-chain PFAS removal was higher in DI than in LW. Indeed, OM competed with short-chain PFAS during adsorption process (Ateia et al., 2018). Overall, lower removal efficiency has been obtained for short-chain PFAS compared with that observed for long-chain ones (removal <20% and >70%, respectively). The effect of different types of NOM (with different hydrophobicity) was also investigated in order to assert the performance of PEI-f-CMC for PFAS removal. The two NOM solutions tested had the same DOC concentration (2 mg L^{-1}) but a different value of specific ultra-violet absorbance at 254 nm ($SUVA_{254}$). Results have

demonstrated that short-chain removal was lower than 30% from both NOM solutions and the competition between short-chain PFAS and hydrophilic NOM ($SUVA_{254}$ = 1.7 L mg^{-1} m^{-1}) was higher than that with hydrophobic NOM ($SUVA_{254}$ = 4.9 L mg^{-1} m^{-1}). The hydrophobicity of NOM does not seem to influence the adsorption of long-chain PFAS on PEI-f-CMC and their removal efficiency was higher than 70% for both NOM solutions.

6. Regeneration of adsorbents

Despite the widespread use of adsorption and anion-exchange processes for PFAS removal, the main drawback of their application at full-scale is the regeneration of spent materials when their adsorption capacity has been exhausted. Regeneration must allow the removal of adsorbed PFAS in order to restore the adsorption capacity of spent materials by means of technologies, which have economic viability and environmental security.

For instance, chemical regeneration of saturated adsorbents is usually performed in situ at full scale treatment processes. However, it is not always feasible because of the related costs or environmental issues, as discussed in the next section. On the other hand, the thermal regeneration is often performed off-site at the adsorbent manufacturing establishment. Therefore, a direct comparison between the above-mentioned techniques is not easy. Overall, in-situ regeneration should be pursued to avoid the transportation, treatment and/or disposal of exhausted materials.

To date, regeneration and reuse of materials saturated with PFAS is challenging, as discussed in the following sections.

6.1. Chemical regeneration

PFAS anionic head could be desorbed using a solution of sodium salts (such as sodium chloride, NaCl, and sodium hydroxide, NaOH), whereas a solution of organic alcohol is required to desorb the hydrophobic C-F chain (Wang et al., 2014; Woodard et al., 2017). Figure 4 depicts a schematic view of PFAS-saturated adsorbent which is regenerated using a chemical solution made of sodium salts and organic alcohol. In Figure 3 the desorption mechanisms related to the use of sodium ions and organic solvents are illustrated as well.

Table 5 reports a compilation of data on chemical regeneration of PFAS-exhausted adsorbents with particular attention to chemical solution employed and regeneration percentage achieved. Due to the lower solubility of PFAS on ionic strength media, conventional solutions of sodium salts were ineffective in regenerating adsorbents exhausted by both long- and short-chain PFAS (Conte et al., 2015; Deng et al., 2015b). Regeneration percentages were lower than 10% when regeneration agents, including NaCl and NaOH, were adopted for desorbing PFBS and PFOS from acrylic resins (Carter and Farrell, 2010; Deng et al., 2010). The deprotonation of amine groups on acrylic gel-type resins allowed the desorption of PFOS at a low concentration of NaOH solutions, although a regeneration percentage of about 90% was achieved when a solution of sodium hydroxide and methanol was tested (Table 5).

Mixture of sodium salts and organic solvents (such as CH_3OH, C_2H_5OH and C_3H_6O) have been widely used in order to involve the desorption of PFAS (Deng et al., 2015b; Yu et al., 2008; Zaggia et al., 2016). Moreover, the efficiency of regenerating solution depends on resin properties and, in particular, on the interactions established between PFAS and resin functional groups (Deng et al., 2010). In fact, data from regeneration

1004 experiments carried out using different mixtures of inorganic salts with or without
1005 organic alcohol demonstrated that the amount of PFAS desorbed from three different
1006 types of strong AE resins depends on resin hydrophobicity and, consequently, on the
1007 interactions between PFAS and the alkyl chains of the functional exchange group
1008 (Zaggia et al., 2016). Solution of ammonium salts (such as NH_4OH and NH_4Cl) showed
1009 a good efficiency for the desorption of PFBA, PFBS, PFOA and PFOS from AE resins
1010 with trimethyl quaternary amine functional group (i.e., Purolite A600E and A520E).
1011 Whereas, the same regenerating solution was totally ineffective in reactivating highly
1012 hydrophobic resin (i.e., Purolite A532E), since the solvatation of fluorine chain was
1013 needed in order to remove PFAS molecules from the active sites of the resin (Table 5).
1014 In that case, the organic solvent could slacken the hydrophobic interactions between
1015 PFAS and resin, then the inorganic anions of ammonium salts (OH^- or Cl^-) could replace
1016 PFAS (Figure 4), achieving the recovery of the exchange capacity of the resin.
1017 The effect of different temperatures of DI water as regenerating solution on PFOS
1018 desorption from BdAC was also investigated (Deng et al., 2015b). Results from
1019 regeneration experiments demonstrated that a higher temperature of DI water (about 80
1020 °C) enhanced the PFOS desorption and the regeneration percentage was about 53%
1021 (Table 5). Furthermore, PFOS desorption from PACFs was about 5% when DI water
1022 was employed as regenerating solution (Chen et al., 2017). By contrast, the
1023 regeneration percentage increased with the increase of ethanol concentration in the
1024 regeneration solution (Chen et al., 2017; Punyapalakul et al., 2013; Wang et al., 2014).
1025 Nevertheless, regenerating solution made of organic solvent is not suitable for the
1026 treatment of drinking water on full-scale applications, and consequently on-site

regeneration is not feasible. It is noteworthy that the effect of OM co-adsorbed on materials may affect regeneration efficiency. After five successive adsorption-regeneration cycles, the efficiency of BdAC for PFCAs removal (PFHxA, PFHpA and PFOA) decreased, while AE resin (IRA67) performance was relatively stable (Du et al., 2015). Co-adsorbed organic pollutants on surface or pores of AC could interfere with the regeneration process. It was the case of the R-CAC, which was regenerated through different regenerating solutions (made of 70% ethanol, 90% methanol or 90% acetone). After the regeneration, R-CAC was reused for PFOS and F-53B removal from industrial wastewater (Du et al., 2016a). Due to the presence of non-desorbed OM, the adsorption efficiency of regenerated R-CAC decreased after each regeneration cycle. For this reason, persulfate oxidation was tested as alternative regeneration process to the conventional elution with organic solvents. Regeneration results demonstrated that sulphate free radicals were able to diffuse into pores of activated carbon and they allowed the degradation of both PFAS and other organic compounds. However, sulphate free radicals could cause the release of fluorine and short-chained PFAS due to break-down of long-chained PFAS (Du et al., 2016a). Consequently, further investigations should be addressed in order to better understand the effect of sulphate and other free radicals on degradation of PFOS.

Overall, the need of organic solvents for the chemical regeneration of PFAS saturated adsorbents is a relevant limitation of this technique.

6.2. Thermal regeneration

Thermal regeneration in N_2 gas stream of GAC saturated with long-chain PFAS (PFOS, PFHxS and PFOA) has been investigated in order to evaluate the release of volatile organic fluorine (VOF) or other compounds such as short-chain compounds (Watanabe

et al., 2016). Thermal regeneration may be optimized when GAC is maintained at 700 °C and later off-gases will be kept at 1000 °C. Nevertheless, the high temperature needed for thermally regenerating AC may cause the decreasing of their adsorption properties and a change in AC morphology (Watanabe et al., 2018). These described aspect of thermal regeneration of activated carbon deserve a deep investigation. Calcination at 600 °C in air for 20 min has been investigated for the reusability of h-BNs saturated with PFDA and PFOS (Feng et al., 2016). A temperature of 600 °C was selected in order to reach the complete decomposition of the investigated PFAS compounds, since PFOS and PFDA are decomposed at about 480 °C and 200 °C, respectively, as inferred from differential scanning calorimetry curves (Feng et al., 2016). Moreover, calcium hydroxide ($Ca(OH)_2$) was employed as additive to avoid the formation of short-chain fluorinated gases during calcination process. Results about regeneration experiments of h-BNs via calcining demonstrated that adsorption capacity was maintained approximately constant during different adsorption-regeneration cycles (the amount of PFOS or PFDA on the surface of h-BNs at equilibrium ranged about 0.35 – 0.45 mg m^{-2}) (Feng et al., 2016).

Recently, microwave (MW) irradiation became an alternative process to conventional thermal regeneration due to its advantages, such as rapidity and selectivity heating (Falciglia et al., 2018). This technique includes the conversion of MW electric field energy adsorbed by the solid medium (i.e., activated carbon) into heat at the molecular level (Falciglia et al., 2017). The dielectric properties of activated carbon combined with PFAS properties (such as their volatility) could allow the regeneration of PFAS-

1073 exhausted AC by means of the interactions between delocalized π-electrons of AC and
1074 the MWs. MW regeneration of PFAS-exhausted AC deserve further investigation.

7. Conclusions and future research recommended

7.1. Conclusions

Poly- and perfluoroalkyl substances (PFAS) are a large group of manmade chemicals characterized by high stability and persistence on environmental compartments. Among interim response measures, adsorption technologies (i.e., by activated carbon or anion-exchange resin) are currently employed for treatment of PFAS-impacted water.

The present critical review of data on PFAS adsorption suggests that:

- To date, most of the experimental works published have been carried out under unrealistic operating conditions, such as high dosage of adsorbent materials, long EBCT, acid pH, and high concentrations of PFAS spiked in DI water. Such conditions are not representative of either full-scale treatment plants or actual environmental contaminations.
- Long-chain PFAS adsorption can involve the formation of aggregates on surface materials that may improve the adsorption efficiency by hydrophobic interactions. Furthermore, when different long-chain PFAS co-exist in solution, the longest PFAS outcompete the shorter due to a stronger hydrophobic interaction between the longest PFAS and the adsorbent surface.
- Meso- and macro-porous adsorbents (both AC and resin) showed high adsorption capacity because long-chain PFAS can easily access.
- Anion-exchange resins are more effective than activated carbon for both long- and short-chain PFAS removal.
- Regardless of the adsorbent used, the adsorption capacity of short-chain PFAS is lower than that observed for long-chain PFAS. Therefore, short-chain PFAS removal is more challenging.

- Adsorption of short-chain PFAS seems related to the availability of active pore sites because the formation of micelles (multi-layer adsorption) does not occur.
- Studies focused on the effect of OM during adsorption process report contrasting results. Overall, co-existing OM negatively affects short-chain PFAS adsorption due to active site competition, whereas the effect of OM seems less relevant during long-chain PFAS adsorption.
- Due to pore blockage and electrostatic repulsions, negative effect of OM on other adsorbent materials (such as biochar, mineral materials and magnetic-nanoparticles) is also reported.
- Effect of co-existing OM should be taken into account during both adsorption and regeneration processes.
- Chemical regeneration of PFAS saturated adsorbents requires the use of organic solvents, which are harmful. Nevertheless, thermal regeneration at high temperature of exhausted activated carbon causes the decline of adsorption capacity and may release dangerous short-chain fluorinated gases. Overall, the in-situ implementation of either chemical or thermal regeneration is not feasible.

7.2. Research needs

The following specific research needs can be drawn based on the observed gaps in PFAS removal by adsorption:

- The investigation of PFAS removal by adsorption (especially short-chain PFAS) under typical water treatment conditions (i.e., adsorbent dose or EBCT, pH, PFAS concentrations) is strongly advised.
- An advanced characterization of OM before and after the adsorption processes is also advised. In particular, fractionation of OM measuring hydrophobic,

transphilic and hydrophilic fractions as well as acid, neutral and base fractions is relevant to better understand the adsorption mechanism and the effect of OM. Size exclusion chromatography (SEC) is also suggested to ascertain the effect of molecular weight of OM.

- Characterization of adsorbent morphology by means of transmission electron microscopy, scanning electron microscopy and Fourier transform infrared spectroscopy before and after PFAS uptake is also useful.
- The simultaneous effect of ionic strength and OM should be considered during PFAS adsorption and further investigations are required in order to better understand the contribution of ionic OM and inorganic ions (i.e., monovalent and divalent cations) on PFAS removal. Further experimental works should be performed at different OM fractions but at the same ionic strength in order minimize the possible effect of inorganic ions.
- Economic assessment of PFAS removal techniques should also address the adsorbent disposal/regeneration. For instance, the management of the eluate produced by chemical regeneration of the resins should be considered.
- Other unconventional techniques, such as microwave irradiation, may help to overcome issues concerning the regeneration of PFAS-saturated adsorbents.
- A novel treatment train, which allows the combination of separation and destructive technologies is expected for the sustainable removal of PFAS.

Acknowledgements

1145 This study was partially funded by the University of Catania within the “Piano della
1146 Ricerca Dipartimentale 2016-2018” of the Department of Civil Engineering and
1147 Architecture, Project “Advanced treatment processes for the removal of emerging
1148 contaminants from water (PACEm)”.

References

Ahrens, L., 2011. Polyfluoroalkyl compounds in the aquatic environment: A review of their occurrence and fate. J. Environ. Monit. 13, 20–31. https://doi.org/10.1039/c0em00373e

Appleman, T.D., Dickenson, E.R. V, Bellona, C., Higgins, C.P., 2013. Nanofiltration and granular activated carbon treatment of perfluoroalkyl acids. J. Hazard. Mater. 260, 740–746. https://doi.org/10.1016/j.jhazmat.2013.06.033

Appleman, T.D., Higgins, C.P., Quiñones, O., Vanderford, B.J., Kolstad, C., Zeigler-Holady, J.C., Dickenson, E.R.V., 2014. Treatment of poly- and perfluoroalkyl substances in U.S. full-scale water treatment systems. Water Res. 51, 246–255. https://doi.org/10.1016/j.watres.2013.10.067

Arvaniti, O.S., Stasinakis, A.S., 2015. Review on the occurrence, fate and removal of perfluorinated compounds during wastewater treatment. Sci. Total Environ. 524–525, 81–92. https://doi.org/10.1016/j.scitotenv.2015.04.023

Ateia, M., Attia, M.F., Maroli, A., Tharayil, N., Alexis, F., Whitehead, D.C., Karanfil, T., 2018. Rapid Removal of Poly- and Perfluorinated Alkyl Substances by Poly(ethylenimine)-Functionalized Cellulose Microcrystals at Environmentally Relevant Conditions. Environ. Sci. Technol. Lett. 5, 764–769. https://doi.org/10.1021/acs.estlett.8b00556

Ateia, M., Maroli, A., Tharayil, N., Karanfil, T., 2019. The overlooked short- and ultrashort-chain poly- and perfluorinated substances: A review. Chemosphere 220, 866–882. https://doi.org/10.1016/j.chemosphere.2018.12.186

Brendel, S., Fetter, É., Staude, C., Vierke, L., Biegel-Engler, A., 2018. Short-chain perfluoroalkyl acids: environmental concerns and a regulatory strategy under REACH. Environ. Sci. Eur. 30. https://doi.org/10.1186/s12302-018-0134-4

Buck, R.C., Franklin, J., Berger, U., Conder, J.M., Cousins, I.T., Voogt, P. De, Jensen, A.A., Kannan, K., Mabury, S.A., van Leeuwen, S.P.J., 2011. Perfluoroalkyl and polyfluoroalkyl substances in the environment: Terminology, classification, and origins. Integr. Environ. Assess. Manag. 7, 513–541. https://doi.org/10.1002/ieam.258

Carter, K.E., Farrell, J., 2010. Removal of perfluorooctane and perfluorobutane sulfonate from water via carbon adsorption and ion exchange. Sep. Sci. Technol. 45, 762–767. https://doi.org/10.1080/01496391003608421

Chen, H., Reinhard, M., Nguyen, V.T., Gin, K.Y.H., 2016. Reversible and irreversible sorption of perfluorinated compounds (PFCs) by sediments of an urban reservoir. Chemosphere 144, 1747–1753. https://doi.org/10.1016/j.chemosphere.2015.10.055

Chen, W., Zhang, X., Mamadiev, M., Wang, Z., 2017. Sorption of perfluorooctane sulfonate and perfluorooctanoate on polyacrylonitrile fiber-derived activated carbon fibers: In comparison with activated carbon. RSC Adv. 7, 927–938. https://doi.org/10.1039/c6ra25230c

Chen, X., Xia, X., Wang, X., Qiao, J., Chen, H., 2011. A comparative study on sorption of perfluorooctane sulfonate (PFOS) by chars, ash and carbon nanotubes. Chemosphere 83, 1313–1319. https://doi.org/10.1016/j.chemosphere.2011.04.018

Chularueangaksorn, P., Tanaka, S., Fujii, S., Kunacheva, C., 2014. Adsorption of perfluorooctanoic acid (PFOA) onto anion exchange resin, non-ion exchange resin, and

granular-activated carbon by batch and column. Desalin. Water Treat. 52, 6542–6548. https://doi.org/10.1080/19443994.2013.815589

Conte, L., Falletti, L., Zaggia, A., Milan, M., 2015. Polyfluorinated Organic Micropollutants Removal from Water by Ion Exchange and Adsorption. Polyfluorinated Org. Micropollutants Remov. from Water by Ion Exch. Adsorpt. 43, 2257–2262. https://doi.org/10.3303/CET1543377

Crawford, N.M., Fenton, S.E., Strynar, M., Hines, E.P., Pritchard, D.A., Steiner, A.Z., 2017. Effects of perfluorinated chemicals on thyroid function, markers of ovarian reserve, and natural fertility. Reprod. Toxicol. 69, 53–59. https://doi.org/10.1016/j.reprotox.2017.01.006

Deng, S., Bei, Y., Lu, X., Du, Z., Wang, B., Wang, Y., Huang, J., Yu, G., 2015a. Effect of co-existing organic compounds on adsorption of perfluorinated compounds onto carbon nanotubes. Front. Environ. Sci. Eng. 9, 784–792. https://doi.org/10.1007/s11783-015-0790-1

Deng, S., Nie, Y., Du, Z., Huang, Q., Meng, P., Wang, B., Huang, J., Yu, G., 2015b. Enhanced adsorption of perfluorooctane sulfonate and perfluorooctanoate by bamboo-derived granular activated carbon. J. Hazard. Mater. 282, 150–157. https://doi.org/10.1016/j.jhazmat.2014.03.045

Deng, S., Niu, L., Bei, Y., Wang, B., Huang, J., Yu, G., 2013. Adsorption of perfluorinated compounds on aminated rice husk prepared by atom transfer radical polymerization. Chemosphere 91, 124–130. https://doi.org/10.1016/j.chemosphere.2012.11.015

Deng, S., Yu, Q., Huang, J., Yu, G., 2010. Removal of perfluorooctane sulfonate from wastewater by anion exchange resins: Effects of resin properties and solution chemistry. Water Res. 44, 5188–5195. https://doi.org/10.1016/j.watres.2010.06.038

Deng, S., Zheng, Y.Q., Xu, F.J., Wang, B., Huang, J., Yu, G., 2012. Highly efficient sorption of perfluorooctane sulfonate and perfluorooctanoate on a quaternized cotton prepared by atom transfer radical polymerization. Chem. Eng. J. 193–194, 154–160. https://doi.org/10.1016/j.cej.2012.04.005

Dewitt, J.C., 2015. Molecular and Integrative Toxicology Toxicological Eff ects of Perfl uoroalkyl and Polyfl uoroalkyl Substances.

Domingo, J.L., Nadal, M., 2017. Per- and polyfluoroalkyl substances (PFASs) in food and human dietary intake: A review of the recent scientific literature. J. Agric. Food Chem. 65, 533–543. https://doi.org/10.1021/acs.jafc.6b04683

Du, Z., Deng, S., Bei, Y., Huang, Q., Wang, B., Huang, J., Yu, G., 2014. Adsorption behavior and mechanism of perfluorinated compounds on various adsorbents - A review. J. Hazard. Mater. 274, 443–454. https://doi.org/10.1016/j.jhazmat.2014.04.038

Du, Z., Deng, S., Chen, Y., Wang, B., Huang, J., Wang, Y., Yu, G., 2015. Removal of perfluorinated carboxylates from washing wastewater of perfluorooctanesulfonyl fluoride using activated carbons and resins. J. Hazard. Mater. 286, 136–143. https://doi.org/10.1016/j.jhazmat.2014.12.037

Du, Z., Deng, S., Liu, D., Yao, X., Wang, Yu, Lu, X., Wang, B., Huang, J., Wang, Yujue, Xing, B., Yu, G., 2016a. Efficient adsorption of PFOS and F53B from chrome plating wastewater and their subsequent degradation in the regeneration process. Chem. Eng. J. 290, 405–413. https://doi.org/10.1016/j.cej.2016.01.077

Du, Z., Deng, S., Zhang, S., Wang, B., Huang, J., Wang, Y., Yu, G., Xing, B., 2016b. Selective and high sorption of perfluorooctanesulfonate and perfluorooctanoate by fluorinated alkyl chain modified montmorillonite. J. Phys. Chem. C 120, 16782–16790.

https://doi.org/10.1021/acs.jpcc.6b04757

Eschauzier, C., Beerendonk, E., Scholte-Veenendaal, P., De Voogt, P., 2012. Impact of Treatment Processes on the Removal of Perfluoroalkyl Acids from the Drinking Water Production Chain. Environ. Sci. Technol. 46, 1708–1715. https://doi.org/10.1021/es201662b

Falciglia, P.P., Malarbì, D., Maddalena, R., Greco, V., Vagliasindi, F.G.A., 2017. Remediation of Hg-contaminated marine sediments by simultaneous application of enhancing agents and microwave heating (MWH). Chem. Eng. J. 321, 1–10. https://doi.org/10.1016/j.cej.2017.03.097

Falciglia, P.P., Roccaro, P., Bonanno, L., De Guidi, G., Vagliasindi, F.G.A., Romano, S., 2018. A review on the microwave heating as a sustainable technique for environmental remediation/detoxification applications. Renew. Sustain. Energy Rev. 95, 147–170. https://doi.org/10.1016/j.rser.2018.07.031

Feng, Y., Zhou, Y., Lee, P.H., Shih, K., 2016. Mineralization of perfluorooctanesulfonate (PFOS) and perfluorodecanoate (PFDA) from aqueous solution by porous hexagonal boron nitride: adsorption followed by simultaneous thermal decomposition and regeneration. RSC Adv. 6, 113773–113780. https://doi.org/10.1039/C6RA15564B

Gao, Y., Deng, S., Du, Z., Liu, K., Yu, G., 2017. Adsorptive removal of emerging polyfluoroalky substances F-53B and PFOS by anion-exchange resin: A comparative study. J. Hazard. Mater. 323, 550–557. https://doi.org/10.1016/j.jhazmat.2016.04.069

Guo, H., Liu, Y., Ma, W., Yan, L., Li, K., Lin, S., 2018. Surface molecular imprinting on carbon microspheres for fast and selective adsorption of perfluorooctane sulfonate. J. Hazard. Mater. 348, 29–38. https://doi.org/10.1016/j.jhazmat.2018.01.018

Guo, W., Huo, S., Feng, J., Lu, X., 2017. Adsorption of perfluorooctane sulfonate (PFOS) on corn straw-derived biochar prepared at different pyrolytic temperatures. J. Taiwan Inst. Chem. Eng. 78, 265–271. https://doi.org/10.1016/j.jtice.2017.06.013

Hansen, M.C., Børresen, M.H., Schlabach, M., Cornelissen, G., 2010. Sorption of perfluorinated compounds from contaminated water to activated carbon. J. Soils Sediments 10, 179–185. https://doi.org/10.1007/s11368-009-0172-z

Higgins, C.P., Luthy, R.G., 2006. Sorption of perfluorinated surfactants on sediments. Environ. Sci. Technol. 40, 7251–7256. https://doi.org/10.1021/es061000n

Hölzer, J., Göen, T., Rauchfuss, K., Kraft, M., Angerer, J., Kleeschulte, P., Wilhelm, M., 2009. One-year follow-up of perfluorinated compounds in plasma of German residents from Arnsberg formerly exposed to PFOA-contaminated drinking water. Int. J. Hyg. Environ. Health 212, 499–504. https://doi.org/10.1016/j.ijheh.2009.04.003

Hu, X.C., Andrews, D.Q., Lindstrom, A.B., Bruton, T.A., Schaider, L.A., Grandjean, P., Lohmann, R., Carignan, C.C., Blum, A., Balan, S.A., Higgins, C.P., Sunderland, E.M., 2016. Detection of Poly- and Perfluoroalkyl Substances (PFASs) in U.S. Drinking Water Linked to Industrial Sites, Military Fire Training Areas, and Wastewater Treatment Plants. Environ. Sci. Technol. Lett. 3, 344–350. https://doi.org/10.1021/acs.estlett.6b00260

Inyang, M., Dickenson, E.R.V., 2017. The use of carbon adsorbents for the removal of perfluoroalkyl acids from potable reuse systems. Chemosphere 184, 168–175. https://doi.org/10.1016/j.chemosphere.2017.05.161

ITRC, 2017. Naming Conventions and Physical and Chemical Properties of Per-and Polyfluoroalkyl Substances (PFAS) 1–15. https://doi.org/10.1002/ieam.258

1281 Kaboré, H.A., Vo Duy, S., Munoz, G., Méité, L., Desrosiers, M., Liu, J., Sory, T.K., Sauvé, S.,
1282 2018. Worldwide drinking water occurrence and levels of newly-identified perfluoroalkyl
1283 and polyfluoroalkyl substances. Sci. Total Environ. 616–617, 1089–1100.
1284 https://doi.org/10.1016/j.scitotenv.2017.10.210

1285 Karoyo, A.H., Wilson, L.D., 2016. Investigation of the Adsorption Processes of Fluorocarbon
1286 and Hydrocarbon Anions at the Solid-Solution Interface of Macromolecular Imprinted
1287 Polymer Materials. J. Phys. Chem. C 120, 6553–6568.
1288 https://doi.org/10.1021/acs.jpcc.5b12246

1289 Kothawala, D.N., Köhler, S.J., Östlund, A., Wiberg, K., Ahrens, L., 2017. Influence of dissolved
1290 organic matter concentration and composition on the removal efficiency of perfluoroalkyl
1291 substances (PFASs) during drinking water treatment. Water Res. 121, 320–328.
1292 https://doi.org/10.1016/j.watres.2017.05.047

1293 Kucharzyk, K.H., Darlington, R., Benotti, M., Deeb, R., Hawley, E., 2017. Novel treatment
1294 technologies for PFAS compounds: A critical review. J. Environ. Manage. 204, 757–764.
1295 https://doi.org/10.1016/j.jenvman.2017.08.016

1296 Li, X., Chen, S., Quan, X., Zhang, Y., 2011. Enhanced adsorption of PFOA and PFOS on
1297 multiwalled carbon nanotubes under electrochemical assistance. Environ. Sci. Technol. 45,
1298 8498–8505. https://doi.org/10.1021/es202026v

1299 Liang, X., Gondal, M.A., Chang, X., Yamani, Z.H., Li, N., Lu, H., Ji, G., 2011. Facile preparation
1300 of magnetic separable powdered-activated-carbon/Ni adsorbent and its application in
1301 removal of perfluorooctane sulfonate (PFOS) from aqueous solution. J. Environ. Sci. Heal.
1302 - Part A Toxic/Hazardous Subst. Environ. Eng. 46, 1482–1490.
1303 https://doi.org/10.1080/10934529.2011.609066

1304 Liu, L., Liu, Y., Li, C., Ji, R., Tian, X., 2018. Improved sorption of perfluorooctanoic acid on
1305 carbon nanotubes hybridized by metal oxide nanoparticles. Environ. Sci. Pollut. Res. 25,
1306 15507–15517. https://doi.org/10.1007/s11356-018-1728-5

1307 Llorca, M., Schirinzi, G., Martínez, M., Barceló, D., Farré, M., 2018. Adsorption of perfluoroalkyl
1308 substances on microplastics under environmental conditions. Environ. Pollut. 235, 680–
1309 691. https://doi.org/10.1016/j.envpol.2017.12.075

1310 Lu, X., Deng, S., Wang, B., Huang, J., Wang, Y., Yu, G., 2016. Adsorption behavior and
1311 mechanism of perfluorooctane sulfonate on nanosized inorganic oxides. J. Colloid Interface
1312 Sci. 474, 199–205. https://doi.org/10.1016/j.jcis.2016.04.032

1313 Luo, Q., Zhao, C., Liu, G., Ren, H., 2016. A Porous Aromatic Framework Constructed from
1314 Benzene Rings Has a High Adsorption Capacity for Perfluorooctane Sulfonate. Sci. Rep. 6,
1315 1–9. https://doi.org/10.1038/srep20311

1316 Maimaiti, A., Deng, S., Meng, P., Wang, W., Wang, B., Huang, J., Wang, Y., Yu, G., 2018.
1317 Competitive adsorption of perfluoroalkyl substances on anion exchange resins in simulated
1318 AFFF-impacted groundwater. Chem. Eng. J. 348, 494–502.
1319 https://doi.org/https://doi.org/10.1016/j.cej.2018.05.006

1320 McCleaf, P., Englund, S., Östlund, A., Lindegren, K., Wiberg, K., Ahrens, L., 2017. Removal
1321 efficiency of multiple poly- and perfluoroalkyl substances (PFASs) in drinking water using
1322 granular activated carbon (GAC) and anion exchange (AE) column tests. Water Res. 120,
1323 77–87. https://doi.org/10.1016/j.watres.2017.04.057

1324 Munoz, G., Labadie, P., Botta, F., Lestremau, F., Lopez, B., Geneste, E., Pardon, P., Dévier,
1325 M.H., Budzinski, H., 2017. Occurrence survey and spatial distribution of perfluoroalkyl and
1326 polyfluoroalkyl surfactants in groundwater, surface water, and sediments from tropical

environments. Sci. Total Environ. 607–608, 243–252. https://doi.org/10.1016/j.scitotenv.2017.06.146

Nzeribe, B.N., Crimi, M., Mededovic Thagard, S., Holsen, T.M., 2019. Physico-Chemical Processes for the Treatment of Per- And Polyfluoroalkyl Substances (PFAS): A review. Crit. Rev. Environ. Sci. Technol. 49, 866–915. https://doi.org/10.1080/10643389.2018.1542916

Ochoa-Herrera, V., Sierra-Alvarez, R., 2008. Removal of perfluorinated surfactants by sorption onto granular activated carbon, zeolite and sludge. Chemosphere 72, 1588–1593. https://doi.org/10.1016/j.chemosphere.2008.04.029

OECD/UNEP Global PFC Group, 2013. United Nations Environment Programme: Synthesis paper on per- and polyfluorinated chemicals (PFCs), Environment, Health and Safety, Environment Directorate, OECD. IOMC Inter-Organization Program. Sound Manag. Chem. 1–58.

Pramanik, B.K., Pramanik, S.K., Sarker, D.C., Suja, F., 2017. Removal of emerging perfluorooctanoic acid and perfluorooctane sulfonate contaminants from lake water. Environ. Technol. (United Kingdom) 38, 1937–1942. https://doi.org/10.1080/09593330.2016.1240716

Pramanik, B.K., Pramanik, S.K., Suja, F., 2015. A comparative study of coagulation, granular- and powdered-activated carbon for the removal of perfluorooctane sulfonate and perfluorooctanoate in drinking water treatment. Environ. Technol. (United Kingdom) 36, 2610–2617. https://doi.org/10.1080/09593330.2015.1040079

Punyapalakul, P., Suksomboon, K., Prarat, P., Khaodhiar, S., 2013. Effects of Surface Functional Groups and Porous Structures on Adsorption and Recovery of Perfluorinated Compounds by Inorganic Porous Silicas. Sep. Sci. Technol. 48, 775–788. https://doi.org/10.1080/01496395.2012.710888

Qian, J., Shen, M., Wang, P., Wang, C., Hu, J., Hou, J., Ao, Y., Zheng, H., Li, K., Liu, J., 2017. Co-adsorption of perfluorooctane sulfonate and phosphate on boehmite: Influence of temperature, phosphate initial concentration and pH. Ecotoxicol. Environ. Saf. 137, 71–77. https://doi.org/10.1016/j.ecoenv.2016.11.026

Quiñones, O., Snyder, S.A., 2009. Occurrence of perfluoroalkyl carboxylates and sulfonates in drinking water utilities and related waters from the United States. Environ. Sci. Technol. 43, 9089–9095. https://doi.org/10.1021/es9024707

Rahman, M.F., Peldszus, S., Anderson, W.B., 2014. Behaviour and fate of perfluoroalkyl and polyfluoroalkyl substances (PFASs) in drinking water treatment: A review. Water Res. 50, 318–340. https://doi.org/10.1016/j.watres.2013.10.045

Rattanaoudom, R., Visvanathan, C., Boontanon, S.K., 2012. Removal of concentrated PFOS and PFOA in synthetic industrial wastewater by powder activated carbon and hydrotalcite. J. Water Sustain. 2, 245–258. https://doi.org/10.11912/jws.2.4.245-258

Rizzo, L., Malato, S., Antakyali, D., Beretsou, V.G., Đolić, M.B., Gernjak, W., Heath, E., Ivancev-Tumbas, I., Karaolia, P., Lado Ribeiro, A.R., Mascolo, G., McArdell, C.S., Schaar, H., Silva, A.M.T., Fatta-Kassinos, D., 2019. Consolidated vs new advanced treatment methods for the removal of contaminants of emerging concern from urban wastewater. Sci. Total Environ. 655, 986–1008. https://doi.org/10.1016/j.scitotenv.2018.11.265

Roccaro, P., Sgroi, M., Vagliasindi, F.G.A., 2013. Removal of xenobiotic compounds from wastewater for environment protection: Treatment processes and costs. Chem. Eng. Trans. 32, 505–510.

1373 Ross, I., McDonough, J., Miles, J., Storch, P., Thelakkat Kochunarayanan, P., Kalve, E., Hurst,
1374 J., S. Dasgupta, S., Burdick, J., 2018. A review of emerging technologies for remediation of
1375 PFASs. Remediation 28, 101–126. https://doi.org/10.1002/rem.21553

1376 Sgroi, M., Anumol, T., Roccaro, P., Vagliasindi, F.G.A., Snyder, S.A., 2018a. Modeling
1377 emerging contaminants breakthrough in packed bed adsorption columns by UV
1378 absorbance and fluorescing components of dissolved organic matter. Water Res. 145,
1379 667–677. https://doi.org/10.1016/j.watres.2018.09.018

1380 Sgroi, M., Vagliasindi, F.G.A., Snyder, S.A., Roccaro, P., 2018b. Chemosphere N - N
1381 itrosodimethylamine (NDMA) and its precursors in water and wastewater : A review on
1382 formation and removal. Chemosphere 191, 685–703.
1383 https://doi.org/10.1016/j.chemosphere.2017.10.089

1384 Shon, H.K., Vigneswaran, S., Snyder, S.A., 2006. Critical Reviews in Environmental Science
1385 and Technology Effluent Organic Matter (EfOM) in Wastewater : Constituents , Effects ,
1386 and Treatment Effluent Organic Matter (EfOM) in Wastewater : Crit. Rev. Environ. Sci.
1387 Technol. 37–41. https://doi.org/10.1080/10643380600580011

1388 Stubleski, J., Salihovic, S., Lind, P.M., Lind, L., Dunder, L., McCleaf, P., Eurén, K., Ahrens, L.,
1389 Svartengren, M., van Bavel, B., Kärrman, A., 2017. The effect of drinking water
1390 contaminated with perfluoroalkyl substances on a 10-year longitudinal trend of plasma
1391 levels in an elderly Uppsala cohort. Environ. Res. 159, 95–102.
1392 https://doi.org/10.1016/j.envres.2017.07.050

1393 Sun, Y., Angelotti, B., Brooks, M., Dowbiggin, B., Evans, P.J., Devins, B., Wang, Z.W., 2018. A
1394 pilot-scale investigation of disinfection by-product precursors and trace organic removal
1395 mechanisms in ozone-biologically activated carbon treatment for potable reuse.
1396 Chemosphere 210, 539–549. https://doi.org/10.1016/j.chemosphere.2018.06.162

1397 Szabo, D., Coggan, T.L., Robson, T.C., Currell, M., Clarke, B.O., 2018. Investigating recycled
1398 water use as a diffuse source of per- and polyfluoroalkyl substances (PFASs) to
1399 groundwater in Melbourne, Australia. Sci. Total Environ. 644, 1409–1417.
1400 https://doi.org/10.1016/j.scitotenv.2018.07.048

1401 Trojanowicz, M., Bojanowska-Czajka, A., Bartosiewicz, I., Kulisa, K., 2018. Advanced
1402 Oxidation/Reduction Processes treatment for aqueous perfluorooctanoate (PFOA) and
1403 perfluorooctanesulfonate (PFOS) – A review of recent advances. Chem. Eng. J. 336, 170–
1404 199. https://doi.org/10.1016/j.cej.2017.10.153

1405 Wang, B., Lee, L.S., Wei, C., Fu, H., Zheng, S., Xu, Z., Zhu, D., 2016. Covalent triazine-based
1406 framework: A promising adsorbent for removal of perfluoroalkyl acids from aqueous
1407 solution. Environ. Pollut. 216, 884–892. https://doi.org/10.1016/j.envpol.2016.06.062

1408 Wang, F., Lu, X., Shih, K.M., Wang, P., Li, X., 2014. Removal of perfluoroalkyl sulfonates
1409 (PFAS) from aqueous solution using permanently confined micelle arrays (PCMAs). Sep.
1410 Purif. Technol. 138, 7–12. https://doi.org/10.1016/j.seppur.2014.09.037

1411 Wang, F., Shih, K., Leckie, J.O., 2015. Effect of humic acid on the sorption of perfluorooctane
1412 sulfonate (PFOS) and perfluorobutane sulfonate (PFBS) on boehmite. Chemosphere 118,
1413 213–218. https://doi.org/10.1016/j.chemosphere.2014.08.080

1414 Wang, W., Xu, Z., Zhang, X., Wimmer, A., Shi, E., Qin, Y., Zhao, X., Zhou, B., Li, L., 2018.
1415 Rapid and efficient removal of organic micropollutants from environmental water using a
1416 magnetic nanoparticles-attached fluorographene-based sorbent. Chem. Eng. J. 343, 61–
1417 68. https://doi.org/10.1016/j.cej.2018.02.101

1418 Wang, Y., Niu, J., Li, Y., Zheng, T., Xu, Y., Liu, Y., 2015. Performance and mechanisms for

removal of perfluorooctanoate (PFOA) from aqueous solution by activated carbon fiber. RSC Adv. 5, 86927–86933. https://doi.org/10.1039/c5ra15853b

Watanabe, N., Takata, M., Takemine, S., Yamamoto, K., 2018. Thermal mineralization behavior of PFOA, PFHxA, and PFOS during reactivation of granular activated carbon (GAC) in nitrogen atmosphere. Environ. Sci. Pollut. Res. 25, 7200–7205. https://doi.org/10.1007/s11356-015-5353-2

Watanabe, N., Takemine, S., Yamamoto, K., Haga, Y., Takata, M., 2016. Residual organic fluorinated compounds from thermal treatment of PFOA, PFHxA and PFOS adsorbed onto granular activated carbon (GAC). J. Mater. Cycles Waste Manag. 18, 625–630. https://doi.org/10.1007/s10163-016-0532-x

Woodard, S., Berry, J., Newman, B., 2017. Ion exchange resin for PFAS removal and pilot test comparison to GAC. Remediation 27, 19–27. https://doi.org/10.1002/rem.21515

Xiao, F., 2017. Emerging poly- and per fl uoroalkyl substances in the aquatic environment : A review of current literature. Water Res. 124, 482–495. https://doi.org/10.1016/j.watres.2017.07.024

Xiao, F., Zhang, X., Penn, L., Gulliver, J.S., Simcik, M.F., 2011. Effects of monovalent cations on the competitive adsorption of perfluoroalkyl acids by kaolinite: Experimental studies and modeling. Environ. Sci. Technol. 45, 10028–10035. https://doi.org/10.1021/es202524y

Xiao, L., Ling, Y., Alsbaiee, A., Li, C., Helbling, D.E., Dichtel, W.R., 2017. β-Cyclodextrin Polymer Network Sequesters Perfluorooctanoic Acid at Environmentally Relevant Concentrations. J. Am. Chem. Soc. 139, 7689–7692. https://doi.org/10.1021/jacs.7b02381

Xiao, X., Ulrich, B.A., Chen, B., Higgins, C.P., 2017. Sorption of Poly- and Perfluoroalkyl Substances (PFASs) Relevant to Aqueous Film-Forming Foam (AFFF)-Impacted Groundwater by Biochars and Activated Carbon. Environ. Sci. Technol. 51, 6342–6351. https://doi.org/10.1021/acs.est.7b00970

Yu, J., Lv, L., Lan, P., Zhang, S., Pan, B., Zhang, W., 2012. Effect of effluent organic matter on the adsorption of perfluorinated compounds onto activated carbon. J. Hazard. Mater. 225–226, 99–106. https://doi.org/10.1016/j.jhazmat.2012.04.073

Yu, Q., Deng, S., Yu, G., 2008. Selective removal of perfluorooctane sulfonate from aqueous solution using chitosan-based molecularly imprinted polymer adsorbents. Water Res. 42, 3089–3097. https://doi.org/10.1016/j.watres.2008.02.024

Yu, Q., Zhang, R., Deng, S., Huang, J., Yu, G., 2009. Sorption of perfluorooctane sulfonate and perfluorooctanoate on activated carbons and resin: Kinetic and isotherm study. Water Res. 43, 1150–1158. https://doi.org/10.1016/j.watres.2008.12.001

Zaggia, A., Conte, L., Falletti, L., Fant, M., Chiorboli, A., 2016. Use of strong anion exchange resins for the removal of perfluoroalkylated substances from contaminated drinking water in batch and continuous pilot plants. Water Res. 91, 137–146. https://doi.org/10.1016/j.watres.2015.12.039

Zhang, Q., Deng, S., Yu, G., Huang, J., 2011. Removal of perfluorooctane sulfonate from aqueous solution by crosslinked chitosan beads: Sorption kinetics and uptake mechanism. Bioresour. Technol. 102, 2265–2271. https://doi.org/10.1016/j.biortech.2010.10.040

Zhao, D., Cheng, J., Vecitis, C.D., Hoffmann, M.R., 2011. Sorption of perfluorochemicals to granular activated carbon in the presence of ultrasound. J. Phys. Chem. A 115, 2250–2257. https://doi.org/10.1021/jp111784k

Zhao, P., Xia, X., Dong, J., Xia, N., Jiang, X., Li, Y., Zhu, Y., 2016. Short- and long-chain

perfluoroalkyl substances in the water, suspended particulate matter, and surface sediment of a turbid river. Sci. Total Environ. 568, 57–65. https://doi.org/10.1016/j.scitotenv.2016.05.221

Zhou, Q., Yu, Q., Zhang, Q., Yu, G., Deng, S., He, H., Huang, J., 2009. Sorption of perfluorooctane sulfonate on organo-montmorillonites. Chemosphere 78, 688–694. https://doi.org/10.1016/j.chemosphere.2009.12.005

Zhou, Yusun, He, Z., Tao, Y., Xiao, Y., Zhou, T., Jing, T., Zhou, Yikai, Mei, S., 2016. Preparation of a functional silica membrane coated on Fe3O4nanoparticle for rapid and selective removal of perfluorinated compounds from surface water sample. Chem. Eng. J. 303, 156–166. https://doi.org/10.1016/j.cej.2016.05.137

Ziska, A.D., Park, M., Anumol, T., Snyder, S.A., 2016. Predicting trace organic compound attenuation with spectroscopic parameters in powdered activated carbon processes. Chemosphere 156, 163–171. https://doi.org/10.1016/j.chemosphere.2016.04.073

Tables

Table 1 Physic-chemical properties of selected PFAS.

Table 2 Batch adsorption experiments of long-chain PFAS fitted by Langmuir model.

Table 3 Batch adsorption experiments of short-chain PFAS fitted by Langmuir model.

Table 4 Experimental studies (both batch and column test) of PFAS adsorption performed in the presence of organic matter.

Table 5 Chemical regeneration of PFAS-saturated materials.

Figures

Figure 1 Box-and-whiskers plot concerning the adsorption capacity of long- and short-chain PFAS on different adsorbent materials (AC: activated carbon; Resin; SM: Synthetized materials).

Figure 2 The main interactions established between OM and PFAS molecules during GAC adsorption. A: pore blockage; B: hydrophobic interaction; C: electrostatic repulsion.

Figure 3 The main interactions established between OM and PFAS molecules during anion-exchange process. B: Hydrophobic interaction; C: Electrostatic repulsion.

Figure 4 Chemical regeneration of PFAS-exhausted **adsorbents** using a solution of sodium salt and organic alcohol.

Table 1 Physic-chemical properties of selected PFAS.

Compound name (CAS No.)	Acronym	Formula	MW g mol^{-1}	Log K_{ow}	Solubility in water (mg L^{-1})	Vapor pressure	pKa	Boiling point (°C)	Melting point (°C)	Density (g cm^{-3})
Perfluoroalkyl carboxylic acids (PFCAs)										
Short-chain (C_4-C_7)										
Perfluorobutanoic acid (375-22-4)	PFBA	C_3F_7COOH	214.039[a]	2.31[b]	2.14 · 10^5 (at 25 °C)[c]	6.38 mm Hg (25° C)[c]	1.07[b]	121[c]	-17.5[c]	1.651[c]
Perfluoropentanoic acid (2706-90-3)	PFPeA	C_4F_9COOH	264.047[a]	3.01[b]	n.a.	n.a.	0.34[b]	n.a.	n.a.	n.a.
Perfluorohexanoic acid (307-24-4)	PFHxA	$C_5F_{11}COOH$	314.054[a]	3.48[d]	15700 (at 25 °C)[d]	198 mm Hg (at 25 °C)[d]	-0.16[d]	157[d]	n.a.	
Perfluoroheptanoic acid (375-85-9)	PFHpA	$C_6F_{13}COOH$	364.062[a]	4.15[d]	3.65 (at 25 °C)[d]	0.133 mm Hg (at 25 °C)[d]	-2.29[d]	175[d]	30[d]	1.792 (at 20 °C)[d]
Long-chain (C_8-C_{14})										
Perfluorooctanoic acid (335-67-1)	PFOA	$C_7F_{15}COOH$	414.07[a]	4.81[d]	2290 (at 24 °C)	3.16 · 10^{-2} mm Hg (at 25 °C)[d]	-0.5 – 4.2[d]	192[d]	54.3[d]	3300 g mL^{-1} (at 24 °C)[d]
Perfluorononanoic acid (375-95-1)	PFNA	$C_8F_{17}COOH$	464.078[a]	5.48[d]	n.a.	8.3 · 10^{-2} mm Hg (at 25 °C)[d]	-0.21[d]	n.a.	n.a.	n.a.
Perfluorodecanoic acid (335-76-2)	PFDA	$C_9F_{19}COOH$	514.086[a]	6.51[b]	n.a.	n.a.	-5.2[b]	217 (at 740 mmHg)[a]	77 – 78[a]	1.707 (at 68 °F)[a]
Perfluoroundecanoic acid (2058-94-8)	PFUnDA	$C_{10}F_{21}COOH$	564.093[a]	7. 21[b]	n.a.	n.a.	-5.2[b]	n.a.	n.a.	n.a.
Perfluorododecanoic acid (307-55-1)	PFDoDA	$C_{11}F_{23}COOH$	614.101[a]	7.92[b]	n.a.	n.a.	-5.2[b]	n.a.	n.a.	n.a.
Perfluorotridecanoic acid (72629-94-8)	PFTrDA	$C_{12}F_{25}COOH$	664.109[a]	8.62[b]	n.a.	n.a.	-5.2[b]	n.a.	n.a.	n.a.
Perfluorotetradecanoic acid (376-06-7)	PFTeDA	$C_{13}F_{27}COOH$	717.117[a]	9.32[b]	n.a.	n.a.	-5.2[b]	n.a.	n.a.	n.a.
Perfluoroalkyl sulfonic acids (PFSAs)										
Short-chain (C_4-C_5)										
Perfluorobutane sulfonic acid (375-73-5)	PFBS	$C_4F_9SO_3H$	300.095[a]	1.82[d]	344 (at 25°C)[d]	2.68 · 10^{-2} mm Hg (at 25 °C)[d]	-3.31[d]	210 – 212[d]	n.a.	1.811 g mL^{-1} (at 25 °C)[d]
Perfluoropentane sulfonic acid (2706-91-4)	PFPeS	$C_5F_{11}SO_3H$	350.102[a]	n.a.	n.a.	n.a.	n.a.	n.a.	n.a.	n.a.
Long-chain (C_6-C_{14})										
Perfluorohexane sulfonic acid (355-46-4)	PFHxS	$C_6F_{13}SO_3H$	400.11[a]	3.16[d]	6.2 (at 25°C)[d]	4.6 · 10^{-3} mm Hg (at 25°C)[d]	0.14[d]	238 - 239[d]	n.a.	1.841 g L^{-1}[d]
Perfluoroheptane sulfonic acid (375-92-8)	PFHpS	$C_7F_{15}SO_3H$	450.118[a]	n.a.	n.a.	n.a.	n.a.	n.a.	n.a.	n.a.
Perfluorooctane sulfonic acid (1763-23-1)	PFOS	$C_8F_{17}SO_3H$	500.126[a]	4.49[d]	3.2 · 10^{-3} (at 25°C)[d]	2 · 10^{-3} mm Hg (at 25°C)[d]	< 1.0[d]	249[d]	n.a.	n.a.
Perfluorononane sulfonic acid (474511-07-4)	PFNS	$C_9F_{19}SO_3H$	549.126[a]	6.13[b]	n.a.	n.a.	-3.24[b]	n.a.	n.a.	n.a.

Table 1 Physic-chemical properties of selected PFAS (continued).

Compound name (CAS No.)	Acronym	Formula	MW g mol^{-1}	Log K_{ow}	Solubility in water (mg L^{-1})	Vapor pressure	pKa	Boiling point (°C)	Melting point (°C)	Density (g cm^{-3})
Perfluoroalkyl sulfonic acids (PFSAs)										
Long-chain (C_6-C_{14})										
Perfluorodecane sulfonic acid (335-77-3)	PFDS	$C_{10}F_{21}SO_3H$	600.141[b]	6.83[b]	n.a.	n.a.	-3.24[b]	n.a.	n.a.	n.a.
Perfluoroundecane sulfonic acid (749786-16-1)	PFUnDS	$C_{11}F_{23}SO_3H$	n.a.	n.a.	n.a.	n.a.	n.a.	n.a.	n.a.	n.a.
Perfluorododecane sulfonic acid (79780-39-5)	PFDoDS	$C_{12}F_{25}SO_3H$	700.157[a]	8.23[b]	n.a.	n.a.	-3.24[b]	n.a.	n.a.	n.a.
Perfluorotridecane sulfonic acid (n.a.)	PFTrDS	$C_{13}F_{27}SO_3H$	n.a.	n.a.	n.a.	n.a.	n.a.	n.a.	n.a.	n.a.
Perfluorotetradecane sulfonic acid (n.a.)	PFTeDS	$C_{14}F_{29}SO_3H$	n.a.	n.a.	n.a.	n.a.	n.a.	n.a.	n.a.	n.a.
Perfluoroalkane sulfonamides (FASAs)										
Perfluorooctane sulfonamide (754-91-6)	FOSA	$C_8H_2F_{17}NO_2S$	499.142[a]	5.8[d]	$8.04 \cdot 10^{-3}$ (at 25°C)[d]	0.31 mm Hg (at 25°C) [d]	3.37[b]	n.a.	n.a.	n.a.
Potassium salt of 6:2 chlorinated polyfluorinated ether sulfonate (73606-19-6)	F-53B	6:2 Cl-PFAES	570.67[f]	4.84[e]	n.a.	n.a.	< 1[e]	n.a.	n.a.	n.a.

n.a. not available, [a]PubChem (URL: https://pubchem.ncbi.nlm.nih.gov); [b]Chemicalize (URL: https://chemicalize.com/#/); [c] Lide (2007); [d] Hazardous Substances Data Bank (HSDB) (URL:https://toxnet.nlm.nih.gov); [e] predicted by software SPARC (Xiao, 2017); [f] (Gao et al., 2017).

Table 2 Batch adsorption experiments of long-chain PFAS fitted by Langmuir model.

Adsorbate		Adsorbent		Water matrix	Experimental setup	Adsorption capacity (mg-PFAS/g-adsorbent)	References
Compound	**$[PFAS]_0$**	**Type and properties**	**Batch dose (mg L^{-1}, except stated otherwise)**				
Activated carbon							
PFOA	15 – 150 mg L^{-1}	**GAC Calgon F400**	1000	DI	T = 30 °C, pH 7.2,	112.1	(Ochoa-Herrera and Sierra-Alvarez, 2008)
	1 – 1000 mg L^{-1}	**PAC**	1000	DI	T = 25 °C, 140 rpm, 48 h	426.49 (1.03 mmol g^{-1})	(Rattanaoudom et al., 2012)
	120 mg L^{-1}	**BdAC** S_{BET} = 2450 m^2 g^{-1} Effective size = 0.6–0.85 mm	200	Actual WW (PFOSF WWW)	T=25 °C, 170 rpm, 48 h, pH 4.0	372.6 (0.9 mmol g^{-1})	(Du et al., 2015)
	0.01 – 100,000 µg L^{-1}	**Biochar HWC** S_{BET} = 453 m^2 g^{-1} pore volume= 0.11 cm^3 g^{-1}	ratio of biochar:PFOA 1:3 mg mL^{-1}	LW (DOC=2 mg L^{-1})	T= 22 °C, 30 d, pH 7.2	41.2	(Inyang and Dickenson, 2017)
				WW (DOC=4.9 mg L^{-1})		31.7	
		Biochar PWC S_{BET} = 413 m^2/g pore volume= 0.10 cm^3/g	ratio of biochar:PFOA 1:3 mg mL^{-1}	LW (DOC=2 mg L^{-1})		41.3	
				WW (DOC=4.9 mg L^{-1})		27.7	
	3.8 – 259 mg L^{-1}	**SWNT** Single walled carbon nanotubes S_{BET} = 468 m^2 g^{-1} pore volume = 0.52 cm^3 g^{-1}	250	DI	Room temperature, 3 d, pH 6	78.67 ± 8.28 (190 ± 20 mmol kg^{-1})	(Wang et al., 2016)
		AC Calgon, microporous S_{BET} = 825 m^2 g^{-1} pore volume = 0.54 cm^3 g^{-1}				194.6 ± 4.14 (470 ± 10 mmol kg^{-1})	
	20 – 250 mg L^{-1}	**PAC** S_{BET} = 812 m^2 g^{-1} micropore area = 466 m^2 g^{-1}	100	DI	T = 25 °C, 150 rpm, 168 h (12 h for PAC)	277.42 (0.67 mmol g^{-1})	(Yu et al., 2009)
		GAC S_{BET} = 712 m^2 g^{-1} micropore area = 313 m^2 g^{-1}				161.48 (0.39 mmol g^{-1})	
	0.05 - 10 mg L^{-1}	**MWNT** S_{BET} = 519.7 m^2 g^{-1}	50	DI	T = 25 °C, pH 6.5	2.69 ± 0.29 (0.0065 ± 0.0007 mmol g^{-1})	(Li et al., 2011)
	20 – 300 mg L^{-1}	**PAC** S_{BET} = 1227.19 m^2 g^{-1}	100	DI	T= 25 °C, 180 rpm, pH 5	202.9 (0.49 mmol g^{-1})	(Chen et al., 2017)
		GAC S_{BET} = 815.34 m^2 g^{-1}				178.05 (0.43 mmol g^{-1})	
PFOS	15 – 150 mg L^{-1}	**GAC Calgon F400**	1000	DI	T = 30 °C, pH 7.2	236.4	(Ochoa-Herrera and Sierra-Alvarez, 2008)
		GAC Calgon F300				196.2	
		GAC Calgon URV-MOD1				211.6	
	1 – 1000 mg L^{-1}	**PAC**	1000	DI	T = 25 °C, 140 rpm, 48 h	440.11 (0.88 mmol g^{-1})	(Rattanaoudom et al., 2012)
	44.1 µg L^{-1}	**R-CAC** S_{BET} = 1125 m^2 g^{-1} pore volume = 0.90 cm^3 g^{-1}	50 - 250	Effluent EWTP	T= 25 °C, 170 rpm, 48 h	0.345 mg g^{-1} (345 µg g^{-1})	(Du et al., 2016a)

Table 2 Batch adsorption experiments of long-chain PFAS fitted by Langmuir model (continued).

Adsorbate		Adsorbent		Water matrix	Experimental setup	Adsorption capacity (mg-PFAS/g-adsorbent)	References
Compound	**$[PFAS]_0$**	**Type and properties**	**Batch dose (mg L^{-1}, except stated otherwise)**				
Activated carbon							
PFOS	20 – 250 mg L^{-1}	**PAC** S_{BET} = 812 m^2 g^{-1} micropore area = 466 m^2 g^{-1}	100	DI	T = 25 °C, 150 rpm, 168 h (12 h for PAC)	520.13 (1.04 mmol g^{-1})	(Yu et al., 2009)
		GAC S_{BET} = 712 m^2 g^{-1} micropore area = 313 m^2 g^{-1}				185.04 (0.37 mmol g^{-1})	
	20 – 300 mg L^{-1}	**PAC** S_{BET} = 1227.19 m^2 g^{-1}	100	DI	T= 25 °C, 180 rpm, pH 5	535.13 (1.07 mmol g^{-1})	(Chen et al., 2017)
		GAC S_{BET} = 815.34 m^2 g^{-1}				390.1 (0.78 mmol g^{-1})	
	0.5 – 10 mg L^{-1}	**Corn-derived-biochar (T=250 °C)** S_{BET} = 2.5 m^2 g^{-1} total pore volume = 0.013 cm^3 g^{-1}	200	DI + 0.01 mol L^{-1} of $CaCl_2$ + 200 mg L^{-1} of NaN_3	T= 25 ± 1 °C, 150 rpm, 48 h, pH 7	135.53	(Guo et al., 2017)
		Corn-derived-biochar (T=400 °C) S_{BET} = 3.75 m^2 g^{-1} total pore volume = 0.017 cm^3 g^{-1}				146.52	
		Corn-derived-biochar (T=550 °C) S_{BET} = 41.10 m^2 g^{-1} total pore volume = 0.043 cm^3 g^{-1}				166.42	
		Corn-derived-biochar (T=700 °C) S_{BET} = 297.58 m^2/g total pore volume = 0.199 cm^3/g				169.90	
	59.9 – 415 mg L^{-1}	**SWNT** S_{BET} = 468 m^2 g^{-1} pore volume = 0.52 cm^3 g^{-1}	250	DI	Room temperature, 3 d, pH 6	560.14 ± 40.01 (1120 ± 80 mmol kg^{-1})	(Wang et al., 2016)
	1 – 500 mg L^{-1}	**SWNT** S_{BET} = 547.2 m^2 g^{-1}	200 - 1200	DI	T= 25 °C, 150 rpm, 2 h, pH 7	712	(Chen et al., 2011)
		MWNT10 S_{BET} = 324.9 m^2 g^{-1}				656	
		MWNT50 S_{BET} = 97.2 m^2 g^{-1}				514	
	59.9 – 415 mg L^{-1}	**AC Calgon** microporous S_{BET} = 825 m^2 g^{-1} pore volume = 0.54 cm^3 g^{-1}	250	DI	Room temperature, 3 d, pH 6	480.12 ± 10 (960 ± 20 mmol kg^{-1})	(Wang et al., 2016)
	0.05 - 10 mg L^{-1}	**MWNT** S_{BET} = 519.7 m^2 g^{-1}	50	DI	T = 25 °C, pH 6.5	5.00 ± 0.5 (0.010 ± 0.001 mmol g^{-1})	(Li et al., 2011)
	30 – 200 mg L^{-1} (30 – 200 ppm)	**PAC** S_{BET} = 1521.85 m^2 g^{-1}	133.3	DI	T= 25 °C, 170 rpm	360.1 (0.72 mmol g^{-1})	(Liang et al., 2011)
		40% Ni-PAC S_{BET} = 947.98 m^2 g^{-1}				355.1 (0.71 mmol g^{-1})	
F-53B	102.9 µg L^{-1}	**R-CAC** S_{BET} = 1750 m^2 g^{-1} pore volume = 1.36 cm^3 g^{-1}	50 - 250	Effluent EWTP	T= 25 °C, 170 rpm, 48 h	1.059 (1059.4 µg g^{-1})	(Du et al., 2016a)

Table 2 Batch adsorption experiments of long-chain PFAS fitted by Langmuir model (continued).

Adsorbate		Adsorbent		Water matrix	Experimental setup	Adsorption capacity (mg-PFAS/g-adsorbent)	References
Compound	$[PFAS]_0$	Type and properties	Batch dose (mg L^{-1})				
Molecularly imprinted polymers							
PFOA	1-12 mg L^{-1}	**DFB-CDP** S_{BET} < 10 m^2 g^{-1}	100	DI	T= 23 °C, 400 rpm, 2 h	34	(L. Xiao et al., 2017)
PFOS	20 – 550 mg L^{-1}	**Chitosan-based MIP**	100	DI	T = 25 °C, 36 h, pH 5	1455.52 (2910.3 µmol g^{-1})	(Yu et al., 2008)
		Chitosan-based NIP				1203.51 (2406.4 µmol g^{-1})	
	10 - 80 mg L^{-1}	**MIP-CMS**	250	DI	T= 25 °C, 150 rpm, 2 h, pH 3	75.99	(Guo et al., 2018)
		NIP-CMS	250			43.94	
Anion-exchange resin							
F-53B	25-400 mg L^{-1}	**IRA67** Polyacrylic-DVB gel-type Polyamine Exchange capacity = 1.6 meq mL^{-1} Effective size = 0.3–1.2 mm	50	Actual WW (chrome plating WW)	T=25 °C, 150 rpm, 48 h, pH 3	2396.84 (4.2 mmol g^{-1})	(Gao et al., 2017)
PFOA	120 mg L^{-1}	**IRA67** Polyacrylic-DVB gel-type Polyamine Exchange capacity = 1.6 meq mL^{-1} Effective size = 0.3 – 1.2 mm	100	Actual WW (PFOSF WWW)	T=25 °C, 170 rpm, 48 h, pH 4.0	1167.67 (2.82 mmol g^{-1})	(Du et al., 2015)
	50 – 400 mg L^{-1}	**IRA910** Polystyrene-DVB macroporous-type Dimethyl ethanol ammonium Exchange capacity = 1.0 meq mL^{-1}	100	DI	T= 25 °C, 160 rpm, 240 h, pH 6	1436.82 (3.47 mmol g^{-1})	(Maimaiti et al., 2018)
	20 – 250 mg L^{-1}	**IRA400** Styrene-DVB gel-type Quaternary ammonium Exchange capacity = 1.4 meq mL^{-1}	100	DI	T = 25 °C, 150 rpm, 168 h	1209.08 (2.92 mmol g^{-1})	(Yu et al., 2009)
	3.8 – 259 mg L^{-1}		375	DI	Room temperature, 3 d, pH 6	331.25 ± 8.28 (800 ± 20 mmol kg^{-1})	(Wang et al., 2016)
PFHxS	50 – 400 mg L^{-1}	**IRA910** Polystyrene-DVB macroporous-type Dimethyl ethanol ammonium Exchange capacity = 1.0 meq mL^{-1}	100	DI	T= 25 °C, 160 rpm, 240 h, pH 6	1364.37 3.41 mmol g^{-1}	(Maimaiti et al., 2018)
PFOS	25-400 mg L^{-1}	**IRA67** Polyacrylic-DVB gel-type Polyamine Exchange capacity = 1.6 meq mL^{-1} Particle size = 16 – 50 mesh	0.05	Actual WW (chrome plating WW)	T=25 °C, 150 rpm, 48 h, pH 3	2750.71 (5.5 mmol g^{-1})	(Gao et al., 2017)
	400 mg L^{-1}		35 - 500	DI		2000.52 – 2500.65 (4 – 5 mmol g^{-1})	(Deng et al., 2010)

Table 2 Batch adsorption experiments of long-chain PFAS fitted by Langmuir model (continued).

Adsorbate		Adsorbent		Water matrix	Experimental setup	Adsorption capacity (mg-PFAS/g-adsorbent)	References
Compound	**$[PFAS]_0$**	**Type and properties**	**Batch dose (mg L^{-1})**				
Anion-exchange resin							
PFOS	400 mg L^{-1}	**IRA958** Polyacrylic macroporous-type Quaternary ammonium Exchange capacity = 3.7 meq g^{-1} Effective size = 0.3 – 1.2 mm	35 - 500	DI	T=25 °C, 150 rpm, 48 h, pH 3	2000.52 – 2500.65 (4 – 5 mmol g^{-1})	(Deng et al., 2010)
	50 – 400 mg L^{-1}	**IRA910** Polystyrene-DVB macroporous-type Dimethyl ethanol ammonium Exchange capacity = 1.0 meq mL^{-1}	100	DI	T= 25 °C, 160 rpm, 240 h, pH 6	1395.36 2.79 mmol g^{-1}	(Maimaiti et al., 2018)
	20 – 250 mg L^{-1}	**IRA400** Styrene-DVB gel-type Quaternary ammonium Exchange capacity = 1.4 meq mL^{-1}	100	DI	T = 25 °C, 150 rpm, 168 h	210.05 (0.42 mmol g^{-1})	(Yu et al., 2009)
	59.9 – 415 mg L^{-1}		375	DI	Room temperature, 3 d, pH 6	165.04 ± 20 (330 ± 40 mmol kg^{-1})	(Wang et al., 2016)
Other materials							
PFOS	15 – 150 mg L^{-1}	**13X zeolite**	1000	DI	T = 30 °C, pH 7.2	12.0	(Ochoa-Herrera and Sierra-Alvarez, 2008)
		NaY80 zeolite				114.7	
	1 – 500 mg L^{-1}	**Chars from maize straw pyrolysis** S_{BET} = 11.6 m^2 g^{-1}	200 - 1200	DI	T= 25 °C, 150 rpm, 384 h, pH 7	164	(Chen et al., 2011)
		Chars from willow sawdust pyrolysis S_{BET} = 7.21 m^2 g^{-1}				91.6	
		MA S_{BET} = 38.3 m^2 g^{-1}				811	
Synthesized materials							
PFDA	0.4 – 50 mg L^{-1}	**h-BNs** S_{BET} = 125.5 m^2 g^{-1} pore volume = 0.915 cm^3 g^{-1}	200	DI	T= 23 ± 2 °C, 150 rpm, 5 mM ammonium acetate	0.16 mg m^{-2}	(Feng et al., 2016)
PFHxS	19.2 – 180 mg L^{-1}	**CTF** S_{BET} = 1270 m^2 g^{-1} pore volume = 0.63 cm^3 g^{-1}	250	DI	Room temperature, 3 d, pH 6	224.06 ± 28 (560 ± 70 mmol kg^{-1})	(Wang et al., 2016)
PFOS	46.51 – 372.1 mg L^{-1}	**Crosslinked chitosan beads** S_{BET} = 14.1 m^2 g^{-1} Particle diameter = 4 – 5 mm	60.8	DI	T= 25 °C, 150 rpm, 150 h, pH 3	2605.67 (5.21 mmol g^{-1})	(Zhang et al., 2011)
	50 – 200 mg L^{-1}	**PAF-45** S_{BET} = 875.38 m^2 g^{-1} pore volume = 0.40 mL g^{-1}	12.5	DI	T= 25 °C, 180 rpm, 48 h, pH 3	5847.39	(Luo et al., 2016)

Table 2 Batch adsorption experiments of long-chain PFAS fitted by Langmuir model (continued).

Adsorbate		Adsorbent		Water matrix	Experimental setup	Adsorption capacity (mg-PFAS/g-adsorbent)	References
Compound	$[PFAS]_0$	Type and properties	Batch dose (mg L^{-1})				
Synthesized materials							
PFOS	0.1 – 250 mg L^{-1}	**ARH**	100	DI	T= 25 °C, 150 rpm, 24 h, pH 5	1325.34 (2.65 mmol g^{-1})	(Deng et al., 2013)
	0.4 – 50 mg L^{-1}	**h-BNs** S_{BET} = 125.5 m^2 g^{-1} pore volume = 0.915 cm^3 g^{-1}	200	DI	T= 25 °C, 180 rpm, 5 mM ammonium acetate	0.04 mg m^{-2}	(Feng et al., 2016)
	59.9 – 415 mg L^{-1}	**CTF** S_{BET} = 1270 m^2 g^{-1} pore volume = 0.63 cm^3 g^{-1}	250	DI	Room temperature, 3 d, pH 6	665.17 ± 40.01 (1330 ± 80 mmol kg^{-1})	(Wang et al., 2016)
	95.02 – 460.12 mg L^{-1}	**Quaternized cotton**	100	DI	T= 25 °C, 150 rpm, 24 h, pH 5	1650.43 (3.3 mmol g^{-1})	(Deng et al., 2012)
	0.5 – 40 mg L^{-1}	**2-MNPs@FG** S_{BET} = 169.85 - 225.42 m^2 g^{-1}	250	DI	220 rpm, 30 min	17.2	(Wang et al., 2018)
	20 – 300 mg L^{-1}	**PACFs** S_{BET} = 1782 m^2 g^{-1}	100	DI	T= 25 °C, 180 rpm, pH 5	760.2 (1.52 mmol g^{-1})	(Chen et al., 2017)
PFOA	3.8 – 259 mg L^{-1}	**CTF** S_{BET} = 1270 m^2 g^{-1} pore volume= 0.63 cm^3 g^{-1}	250	DI	Room temperature, 3 d, pH 6	269.14 (650 ± 30 mmol kg^{-1})	(Wang et al., 2016)
	78.67 – 381 mg L^{-1}	**Quaternized cotton**	100	DI	T= 25 °C, 150 rpm, 24 h, pH 5	1283.61 (3.1 mmol g^{-1})	(Deng et al., 2012)
	0.1 – 207.03 mg L^{-1}	**ARH**	100	DI	T= 25 °C, 150 rpm, 24 h, pH 5	1031.03 (2.49 mmol g^{-1})	(Deng et al., 2013)
	0.5 – 40 mg L^{-1}	**2-MNPs@FG** S_{BET} = 169.85 - 225.42 m^2 g^{-1}	250	DI	220 rpm, 30 min	50.4	(Wang et al., 2018)
	20 – 300 mg L^{-1}	**PACFs** S_{BET} = 1782 m^2 g^{-1}	100	DI	T= 25 °C, 180 rpm, pH 5	302.27 (0.73 mmol g^{-1})	(Chen et al., 2017)
	2 – 50 μg L^{-1}	**PEI-f-CMC** S_{BET} = 7.8 m^2 g^{-1}	10	DI	T= 25±1 °C, 150 rpm, 24 h	2.32	(Ateia et al., 2018)

S_{BET}: BET surface area; DI: Deionized water; PFSOF WWW: Perfluorooctanesulfonyl fluoride washing wastewater; LW: Lake water; EWTP: Electroplating wastewater treatment plant; GAC: Granular activated carbon; PAC: Powdered activated carbon BdAC: Bamboo-derived activated carbon; 40% Ni-PAC: Ni-compounded PAC with Ni loading an amount of ~40 wt%; R-CAC: reactivated coconut shell-based GAC; HWC: Harwood; PWC: Pinewood; SWNT: Single-walled carbon nanotubes; MWNT: Multi-walled carbon nanotubes; DFB-CDP: cross-linked polymer network where β-CD substitutes decafluorobiphenyl (DFB); MIP-CMS: molecularly imprinted carbon microsphere; NIP-CMS: non-imprinted carbon microsphere; MA: Ash from burning maize straw on stainless steel plate; CTF: Covalent triazine-based framework; h-BNs: porous hexagonal boron nitride nanosheets; PAF-45: porous aromatic framework constructed from benzene rings; ARH: Aminated rice husk; 2-MNPs@FG: Magnetic nano-particles attached into fluorographene (mass ratio of MNPs and FG is 3:5); WW: wastewater; PACFs: Polyacrylonitrile fiber (PANF)-derived activated carbon fibers; PEI-f-CMC: Poly(ethylenimine)-functionalized cellulose microcrystals.

Table 3 Batch adsorption experiments of short-chain PFAS fitted by Langmuir model.

Adsorbate		Adsorbent		Water matrix	Experimental setup	Adsorption capacity (mg-PFAS/g-adsorbent)	References
Compound	$[PFAS]_0$	Type and properties	Batch dose (mg L^{-1})				
Activated carbon							
PFBA	6.5 – 204 mg L^{-1}	**AC Calgon** microporous S_{BET} = 825 m^2 g^{-1} pore volume = 0.54 cm^3 g^{-1}	250	DI	Room temperature, 3 d, pH 6	51.36 ± 4.28 (240 ± 20 mmol kg^{-1})	(Wang et al., 2016)
PFHxA	31.4 mg L^{-1}	**BdAC** S_{BET} = 2450 m^2 g^{-1} Effective size = 0.6–0.85 mm	200	Actual WW (PFOSF WWW)	T=25 °C, 170 rpm, 48 h, pH 4	18.84 (0.06 mmol g^{-1})	(Du et al., 2015)
	7.2 – 217 mg L^{-1}	**AC Calgon** microporous S_{BET} = 825 m^2 g^{-1} pore volume = 0.54 cm^3 g^{-1}	250	DI	Room temperature, 3 d, pH 6	235.54 ± 72.23 (750 ± 230 mmol kg^{-1})	(Wang et al., 2016)
PFHpA	40.04 mg L^{-1}	**BdAC** S_{BET} = 2450 m^2 g^{-1} Effective size = 0.6–0.85 mm	200	Actual WW (PFOSF WWW)	T=25 °C, 170 rpm, 48 h, pH 4	65.53 (0.18 mmol g^{-1})	(Du et al., 2015)
PFBS	6 – 247 mg L^{-1}	**AC Calgon** microporous S_{BET} = 825 m^2 g^{-1} pore volume = 0.54 cm^3 g^{-1}	250	DI	Room temperature, 3 d, pH 6	51.01 ± 3 (170 ± 10 mmol kg^{-1})	(Wang et al., 2016)
	15 – 150 mg L^{-1}	**GAC Calgon F400**	1000	DI	T = 30 °C, pH 7.2	98.7	(Ochoa-Herrera and Sierra-Alvarez, 2008)
Anion exchange resin							
PFBA	50 – 400 mg L^{-1}	**IRA910** Polystyrene-DVB macroporous-type Dimethyl ethanol ammonium Exchange capacity = 1.0 meq mL^{-1}	100	DI	T= 25 °C, 160 rpm, 240 h, pH 6	635.69 (2.97 mmol g^{-1})	(Maimaiti et al., 2018)
PFHxA	50 – 400 mg L^{-1}	**IRA910** Polystyrene-DVB macroporous-type Dimethyl ethanol ammonium Exchange capacity = 1.0 meq mL^{-1}	100	DI	T= 25 °C, 160 rpm, 240 h, pH 6	1089.76 (3.47 mmol g^{-1})	(Maimaiti et al., 2018)
	31.4 mg L^{-1}	**IRA67** Polyacrylic-DVB gel-type Polyamine Exchange capacity = 1.6 meq mL^{-1} Effective size = 0.3–1.2 mm	100	Actual WW (PFOSF WWW)	T=25 °C, 170 rpm, 48 h, pH 4	37.68 (0.12 mmol g^{-1})	(Du et al., 2015)
PFHpA	40.04 mg L^{-1}	**IRA67** Polyacrylic-DVB gel-type Polyamine Exchange capacity = 1.6 meq mL^{-1} Effective size = 0.3–1.2 mm	100	Actual WW (PFOSF WWW)	T=25 °C, 170 rpm, 48 h, pH 4	192.95 (0.53 mmol g^{-1})	(Du et al., 2015)
PFBS	50 – 400 mg L^{-1}	**IRA910** Polystyrene-DVB macroporous-type Dimethyl ethanol ammonium Exchange capacity = 1.0 meq mL^{-1}	100	DI	T= 25 °C, 160 rpm, 240 h, pH 6	1023.32 (3.41 mmol g^{-1})	(Maimaiti et al., 2018)

Table 3 Batch adsorption experiments of short-chain PFAS fitted by Langmuir model (continued).

Adsorbate		Adsorbent		Water matrix	Experimental setup	Adsorption capacity (mg-PFAS/g-adsorbent)	References
Compound	$[PFAS]_0$	Type and properties	Batch dose (mg L^{-1})				
Synthesized materials							
PFBA	0.1 – 107.02 mg L^{-1}	**ARH**	100	DI	T= 25 °C, 150 rpm, 24 h, pH 5	363.86 (1.70 mmol g^{-1})	(Deng et al., 2013)
	6.5 – 204 mg L^{-1}	**CTF** S_{BET} = 1270 m^2 g^{-1} pore volume = 0.63 cm^3 g^{-1}	250	DI	Room temperature, 3 d, pH 6	92.03 ± 4.28 (430 ± 20 mmol kg^{-1})	(Wang et al., 2016)
PFHxA	7.2 – 217 mg L^{-1}					376.86 ± 94.21 (1200 ± 300 mmol kg^{-1})	
PFBS	6 – 247 mg L^{-1}					141.04 ± 12 (470 ± 40 mmol kg^{-1})	

AC: activated carbon; S_{BET}: BET surface area; DI: deionized water; PFOSF WWW: perfluorooctanesulfonyl fluoride washing wastewater; GAC: granular activated carbon; BdAC: bamboo-derived activated carbon; ARH: aminated rice husk; CTF: covalent triazine-based framework; WW: wastewater

Table 4 Experimental studies (both batch and column test) of PFAS adsorption performed in the presence of organic matter.

Adsorbate		Adsorbent		Organic matter		Experimental setup	Remarks	References
Target PFAS	**Level**	**Type**	**Batch dose or EBCT**	**Source (Water matrix)**	**Concentration**			
PFOS **PFOA**	200 μg L^{-1} **Spiking** (Single solute)	**PAC**	10 mg L^{-1}	**EfOM** (WWTP effluent)	DOC =7.3 mg L^{-1}	Batch • PFOA or PFOS + EfOM • PFOA or PFOS + PAC loaded of EfOM	PFOA (or PFOS) needs much contact time to reach the equilibrium in the presence of EfOM, in particular onto EfOM-preloaded PAC; EfOM (especially low-molecular-weight compounds) impacts negatively adsorption rate and capacity.	(Yu et al., 2012)
PFBA **PFPeA** **PFHxA** **PFOA** **PFNA** **PFDA** **PFBS** **PFHxS** **PFOS**	1 μg L^{-1} of each PFAS **Spiking** (Mix)	**GAC** (F300, F600, 1240C)	0.38 min	**DOM (SW)** Clear Creek (Golden, CO)	DOC = 1.7 mg L^{-1}	Column RSSCT experiment	The presence of DOM leads to faster breakthrough of PFAS, in particular shortest chain compounds. Breakthrough of >20% for all PFAS tested has been reached at 11,000 BVs and 125,000 BVs, respectively in the presence and absence of DOM. F300 is less effective with PFBA and PFPeA.	(Appleman et al., 2013)
PFOS **PFOA** **PFBS** **PFHxS**	250.06 μg L^{-1} 207.03 μg L^{-1} 150.04 μg L^{-1} 200.05 μg L^{-1} **Spiking** (Single solute)	**MWCNTs** (MWCNTs-Pri MWCNTs-COOH MWCNTs-OH)	20 mg L^{-1}	**Synthetic OM** (HA, 1-naphthol, phenol, benzoic acid) (Sinopharm Chemical Regent) **in DI**	Range of tested concentration of HA, 1-naphtol, phenol and benzoic acid 0 - 2.5 mg L^{-1}	Batch • PFOS + HA (or 1-naphthol, phenol, benzoic acid) • PFBS (or PFHxS, PFOA) + HA or Phenol	Competition between PFAS and organic compounds on the adsorption sites of the MWCNTs; Effect of co-existing organic compounds on PFOS removal: HA > 1-naphtol > benzoic acid > phenol; % removal in the presence of HA or phenol: PFOS > PFOA > PFHxS > PFBS.	(Deng et al., 2015a)
PFOS **F-53B**	44.1 μg L^{-1} 102.9 μg L^{-1} **Real** (Mix)	**R-CAC**	100 mg L^{-1}	**EfOM** (EWTP effluent)	TOC = 78.3 mg L^{-1}	Batch adsorption experiments of actual WW and synthetic PFAS solution (OM free)	EWTP effluent contains high amount of hydrocarbon surfactants (high concentration of TOC) which are in competition with PFOS and F-53B for active sites on R-CAC; F-53B is better adsorbed on R-CAC than PFOS due to its more hydrophobic chain and its higher concentration in the actual wastewater.	(Du et al., 2016a)
PFOS **PFOA**	280 ng L^{-1} 550 ng L^{-1} (read from graph)	**PAC** (BET 880 $m^2 g^{-1}$) **GAC** (BET 800 $m^2 g^{-1}$)	10 min	**Synthetic HA and FA** (Sigma-Aldrich) **in DW**	Range of tested concentration of HA and FA 5 – 25 mg L^{-1}	Column	PAC and GAC efficiencies decrease with the increasing of DOC concentration.	(Pramanik et al., 2015)

Table 4 Experimental studies (both batch and column test) of PFAS adsorption performed in the presence of organic matter (continued).

Adsorbate		Adsorbent		Organic matter		Experimental setup	Remarks	References
Target PFAS	**Level**	**Type**	**Batch dose or EBCT**	**Source (Water matrix)**	**Concentration**			
C_4 – C_{12}, C_{14} PFCAs (PFBA,PFPeA, PFHxA, PFHpA, PFOA, PFNA, PFDA, PFUnDA, PFDoDA, PFTeDA) **C_4, C_6, C_8 PFSAs** (PFBS, PFHxS, PFOS) **FOSA**	0.1 µg L^{-1} **Spiking** (Mix)	**GAC** (F400)	6.1 min	**DOM (DW)**	DOC = 1.8 mg L^{-1}	Column RSSCT experiment	DOC removal is not linked to PFAS removal from AE or GAC column. DOC loading seems to favour the agglomeration of PFAS on the adsorbent surface.	(McCleaf et al., 2017)
		AE resin (A-600, Polystyrene-DVB gel-type Quaternary ammonium)	4.9 min					
PFBS 0.073 ± 0.01 µg L^{-1} **PFHxS** 0.47 ± 0.08 µg L^{-1} **PFOS** 1.4 ± 0.2 µg L^{-1} **PFHxA** 0.28 ± 0.04 µg L^{-1} **PFHpA** 0.32 ± 0.04 µg L^{-1} **PFOA** 1.4 ± 0.13 µg L^{-1} **PFNA** 0.067 ± 0.005 µg L^{-1} **PFDA** 0.04 ± 0.02 µg L^{-1} **Real** (Mix)		**GAC** (coal-based, Silcarbon)	125 mg L^{-1}	**DOM (GW)** (well at 9.5 m depth, downstream a water-resistant clothing manufacture)	DOC = 5.27 ± 0.12 ng L^{-1}	Batch adsorption isotherm for each adsorbent have been measured for the undiluted PFAS contaminated GW	Effect of OM has not been highlighted.	(Hansen et al., 2010)
		PAC (anthracite coal, Silcarbon TH90 extra)	25 mg L^{-1}					
C_4 – C_{12} PFCAs (PFBA, PFPeA, PFHxA, PFHpA, PFOA, PFNA, PFDA, PFUnDA, PFDoDA) **C_4, C_6, C_8 PFSAs** (PFBS, PFHxS, PFOS) **FOSA**	2.5 µg L^{-1} of each PFAS **Spiking** (Mix)	**AE resin** (A600, Polystyrene-DVB gel-type Quaternary ammonium)	10 g L^{-1}	**DOM (LW)** •Görväln (autochtonous DOM, hydrophobic) • Bolmen (terrestrial, algal and bacterial-derived DOM, hydrophilic)	•DOC = 8.3 mg L^{-1} •DOC = 10 mg L^{-1}	Batch Pre-equilibration condition (contact time about 15 min) 4 discrete DOM levels (8, 4, 2, 0 mg DOC L^{-1}) for the two lake waters + PFAS mix	Effect of DOM is weak during PFAS removal by AE, in fact at the highest DOM concentration PFAS percentual removal has been reduced by 10% in comparison with DOC free solution;	(Kothawala et al., 2017)
		GAC (Filtrasorb 400, Calgon)					GAC performance is affected by DOC source and concentration. Most hydrophobic long chain PFAS are better removed at highest DOC concentration, in detail the increase of hydrophobic DOM (Görväln) concentration enhances progressively PFAS removal. Whereas, only the absence or presence of hydrophilic DOM (Bolmen) seems to influence PFAS adsorption.	

Table 4 Experimental studies (both batch and column test) of PFAS adsorption performed in the presence of organic matter (continued).

Adsorbate		Adsorbent		Organic matter		Experimental setup	Remarks	References
Target PFAS	**Level**	**Type**	**Batch dose or EBCT**	**Source (Water matrix)**	**Concentration**			
PFOS **PFOA** **PFDA**	0.153 µg L^{-1} 0.138 µg L^{-1} 0.282 µg L^{-1} **Spiking** (Mix)	**GAC** (Norit Darco 12x40)	5.2 min	**Synthetic NOM** (Suwanne river, International Humic Substances Society) **in DI**	DOC = 4.3 mg L^{-1}	Column RSSCT experiment	Similar breakthrough curves of PFAS tested have been obtained despite different DOM composition and concentration. DOM seems not influenced the amount of long-chained PFAS adsorbed since hydrophobic interaction represents the main adsorption mechanism.	(Sgroi et al., 2018a)
	0.153 µg L^{-1} 0.269 µg L^{-1} 0.238 µg L^{-1} **Spiking** (Mix)			**NOM** (SW)	DOC = 5.4 mg L^{-1}			
	0.556 µg L^{-1} 0.174 µg L^{-1} **Real** (Mix)			**EfOM** (WWTP effluent secondary)	DOC = 7 mg L^{-1}			
PFHxS	200 mg L^{-1} **Spiking**	**AE resin** (IRA910, Polystyrene-DVB macroporous-type Dimethyl ethanol ammonium)	0.1 g L^{-1}	**Synthetic TCE, MB, SDS** (Sinopharm Chemical Reagent) **in DI**	Range of tested concentration of TCE, MB, SDS 0 – 5 mmol L^{-1}	Batch adsorption experiments are carried out by dissolving PFHxS with different organic compounds at varying concentration	Non-ionic co-existing organic compounds (i.e. MB and TCE) do not impacted PFHxS removal, regardless their concentration. Due to the affinity of AE with anionic species, IRA910 performance decreases with the increase of HA and SDS concentrations. In detail, HA and SDS occupies adsorption sites on IRA910 and the latest could form aggregates in competition with PFHxS.	(Maimaiti et al., 2018)
				Synthetic HA (Sinopharm Chemical Reagent) **in DI**	Range of tested concentration of HA 0 – 200 mg L^{-1}			
PFOA	100 mg L^{-1}	**ACF**	800 mg L^{-1}	**Synthetic FA** (Sinopharm Chemical Regent) **in DI**	Range of tested concentration of FA 0 – 500 mg L^{-1}	Batch adsorption experiments at varying FA concentrations are compared with blank experiments (FA free solution)	FA concentration of 100 mg L^{-1} causes a decrease of PFOA adsorbed (about 75.4% lower than that of FA free solution).	(Y. Wang et al., 2015)
PFHxA **PFHpA** **PFOA**	31.4 mg L^{-1} 40.04 mg L^{-1} 120.08 mg L^{-1} **Real** (Mix)	**BdAC**	0.2 g L^{-1}	**DOM** (PFOSF WWW)	TOC = 63.2 mg L^{-1}	Batch adsorption experiments of simulated (DI+PFAS) and actual WW	Co-existing organic matter in actual WW has no effect on PFCAs adsorption on IRA67, whereas their presence influences negatively BdAC efficiency.	(Du et al., 2015)
		AE resin (IRA67, Polyacrylic-DVB gel-type Polyamine)	0.1 g L^{-1}					

Table 4 Experimental studies (both batch and column test) of PFAS adsorption performed in the presence of organic matter (continued).

Adsorbate		Adsorbent		Organic matter		Experimental setup	Remarks	References
Target PFAS	Level	Type	Batch dose or EBCT	Source (Water matrix)	Concentration			
PFOA	1 µg L^{-1} **Spiking**	**DFB-CDP**	10 mg L^{-1}	**Synthetic HA** (n.a.) **in DI**	20 mg L^{-1}	Batch kinetic experiments are performed by adding HA to the adsorbent suspension together with PFOA solution. Comparison between PFOA removal by DFB-CDP in the presence or absence of HA	DFB-CDP adsorption efficiency is unaffected by HA.	(L. Xiao et al., 2017)
PFOS PFBS	50 – 1000 µg L^{-1} **Spiking** (Single compound)	**Boehmite**	5 g L^{-1}	**Synthetic HA** in DI Fluka Co. (Buchs, Switzerland)	Range of tested concentration of HA 2 – 50 mg L^{-1}	Batch adsorption experiments performed for 72 h for achieving the equilibrium	With the increasing of HA adsorbed, boehmite surface becomes negative and electrostatic repulsions cause the reduction in PFOS and PFBS sorption.	(F. Wang et al., 2015)
PFOA PFOS	340 ng L^{-1} 520 ng L^{-1} **Real** (Mix)	**GAC** (BET = 800 m^2 g^{-1})	20 min	**Commercial organics**: BSA, sodium alginate and HA (Sigma-Aldrich) **in LW**	DOC= 7.88 ± 0.07 mg L^{-1} Protein = 11.54 ± 0.22 mg L^{-1} Carbohydrate = 8.92 ± 0.28 mg L^{-1}	Column	Removal efficiency is the highest at the lower DOC concentration, due to the competition for adsorption sites. Protein has the greater influence on PFOA and PFOS adsorption behaviour by means of hydrophobic and electrostatic interactions.	(Pramanik et al., 2017)
PFOA PFOS	103.5 – 4140.7 µg L^{-1} 125 – 5001.2 µgl L^{-1} **Spiking** (Single compound)	**F-MT**	10 mg L^{-1}	**Synthetic HA** (n.a.) **in DI**	Tested concentration of HA 1 and 10 mg L^{-1}	Batch comparison of PFOA and PFOS adsorbed amounts in absence or in presence of HA	Due to nanoscale interlayers and high hydrophobicity of F-MT, HA macromolecular with hydrophilic groups could not be adsorbed. Consequently, co-existing HA weakly interferes with PFOS and PFOA adsorption (little decrease of PFOS and PFOA adsorption appeared in the presence of 10 mg L^{-1} HA).	(Du et al., 2016b)
PFOS PFOA PFBA PFBS	50 mg L^{-1} **Spiking** (Mix)	**GAC** (Filtrasorb 600, Calgon)	400 mg L^{-1}	**DOM** (Landfill GW)	Range of tested concentration of TOC 5-20 mg L^{-1}	Batch adsorption isotherm experiments are conducted on both DI and landfill GW	Organic compounds in groundwater can competitive with PFAS for GAC adsorption sites as it is demonstrated by the great equilibrium and fast kinetic adsorption in DI instead of in the landfill groundwater.	(Zhao et al., 2011)

Table 4 Experimental studies (both batch and column test) of PFAS adsorption performed in the presence of organic matter (continued).

Adsorbate		Adsorbent		Organic matter		Experimental setup	Remarks	References
Target PFAS	**Level**	**Type**	**Batch dose or EBCT**	**Source (Water matrix)**	**Concentration**			
C_4 – C_{14}, C_{16}, C_{18} PFCAs (PFBA, PFPeA PFHxA, PFHpA, PFOA, PFNA, PFDA, PFUnDA, PFDoDA, PFTrDA PFTeDA, PFHxDA, PFODA) **C_4, C_6, C_8, C_{10} PFSAs** (PFBS, PFHxS PFOS, PFDS) **FOSA**	10 µg L^{-1} of each PFAS (∑PFAS=180 µg L^{-1}) **Spiking** (Mix)	**HDPE**	5 mg L^{-1}	**NOM** SeaW (Alfacs Bay) RW (Ebro River)	TOC = 7.735 mg L^{-1} TOC = 4.386 mg L^{-1}	Batch Contact time 0, 4, 7, 50 days	PFAS adsorption on HDPE is influenced by the presence of NOM and this effect is more evidence in seawater where NOM concentration is higher than in river water. Percentages of adsorption on HDPE are below 30% and carboxylic acids are adsorbed better than PFSAs (PFOS and PFDS no adsorption).	(Llorca et al., 2018)
		PS	2 mg L^{-1}				Higher adsorption velocity despite HDPE. Aromatic rings of PS monomer favour PFAS adsorption on PS and they go against organic matter competition.	
		PS-COOH	2 mg L^{-1}				PFAS adsorption on PS-COOH is similar to that on PS, but adsorption rate is lower. C_{11} and C_{18} are the most adsorbed compounds. Effect of NOM not assessed.	
PFOA PFOS	180 µg L^{-1} of each compound **Spiking** (Mix)	**MNPs@FG** (1-MNPs@FG, 2-MNPs@FG, 3-MNPs@FG)	400 mg L^{-1}	**Synthetic NOM** (International Humic Substance Society) **in DI**	DOC = 2 mg L^{-1}	Batch adsorption experiments in orbital shaker at room temperature	The performance of MNPs@FG tested is slightly influenced by the presence of synthetic NOM.	(Wang et al., 2018)
	5 µg L^{-1} of each compound **Spiking** (Mix)	**MNPs@FG** (2-MNPs@FG)	400 mg L^{-1}	**NOM** (LW, RW, DW)	DOC = 1.7 mg L^{-1} DOC = 0.6 mg L^{-1} DOC < 0.1 mg L^{-1}	Batch, investigation of PFOA and PFOS removal from environmental water	After 11 minutes, 2-MNPs@FG exhibits high removal efficiencies (about 99.2 %) for both PFOA and PFOS in all water matrixes tested. The residual concentration of PFOA and PFOS are 11 and 28 ng L^{-1}, 16 and 22 ng L^{-1}, 31 and 18 ng L^{-1}, in lake, river and drinking waters, respectively. Residual combined concentration of PFOA and PFOS (49 ng L^{-1}) in DW is lower than health advisory level of 70 ng L^{-1} (US EPA, 2016)	

Table 4 Experimental studies (both batch and column test) of PFAS adsorption performed in the presence of organic matter (continued).

Adsorbate		Adsorbent		Organic matter		Experimental setup	Remarks	References
Target PFAS	**Level**	**Type**	**Batch dose or EBCT**	**Source (Water matrix)**	**Concentration**			
C_4 – C_8 PFCAs (PFBA, PFPeA PFHxA, PFHpA, PFOA) **C_4 - C_8 PFSAs** (PFBS, PFHxS, PFHpS, PFOS)	3.7 ± 0.9 µg L^{-1} 5.2 ± 0.4 µg L^{-1} 7.6 ± 0.5 µg L^{-1} 1.5 ± 0.1 µg L^{-1} 10.7 ± 0.9 µg L^{-1} 1.8 ± 0.0 µg L^{-1} 21.0 ± 0.3 µg L^{-1} 1.7 ± 0.1 µg L^{-1} 33.1 ± 0.6 µg L^{-1} **Real** (Mix)	**GAC** (Filtrasorb 300, Calgon)	100 mg L^{-1}	**DOM** (AFFF-impacted GW)	DOC = 46.0 ± 0.9 mg L^{-1}	Batch adsorption experiments with unfiltered AFFF-impacted GW for 5 days (no equilibrium reached)	Effect of OM has not been highlighted.	(X. Xiao et al., 2017)
		Biochar (Mountain Crest Gardens, MCG, pine needle-derived biochar)						
PFOA PFOS	82.8 mg L^{-1} 129.12 mg L^{-1} **Spiking** (Single compound)	**CTF**	250 mg L^{-1}	**Synthetic HA** (soil-extracted) **in DI**	Range of tested concentration of HA 10 – 40 mg L^{-1}	Batch single-point adsorption data (equilibrium pH equal to 6) of each chemical testing the different adsorbent materials	HA do not strongly interfere with CTF adsorption since HA molecules are unable to enter in the internal pores of CTF due to size-exclusion mechanism.	(Wang et al., 2016)
		AE resin (IRA-400, Amberlite Sinopharm Chemical Regent Co., China)	375 mg L^{-1}				HA present slightly increases PFOA and PFOS adsorbed rates, maybe due to a weak expansion of the polymer matrix and consequently an increase of PFOA and PFOS access to more adsorption sites.	
		Microporous AC (Calgon Carbon Co., USA)	250 mg L^{-1}				Direct competition for adsorption sites on AC and SWNT between dissolved HA and PFOA or PFOS. At the highest concentration of HA (40 mg L^{-1}), the reduction of PFOA and PFOS adsorption rates are 31-48 % and 95% for both AC and SWNT, respectively.	
		SWNT (Nanotech Port Co., China)	250 mg L^{-1}					

Table 4 Experimental studies (both batch and column test) of PFAS adsorption performed in the presence of organic matter (continued).

Adsorbate		Adsorbent		Organic matter		Experimental setup	Remarks	References
Target PFAS	**Level**	**Type**	**Batch dose or EBCT**	**Source (Water matrix)**	**Concentration**			
C_4 – C_{14} PFCAs (PFBA, PFPeA PFHxA, PFHpA, PFOA, PFNA, PFDA, PFUnDA, PFDoDA) **C_4, C_6, C_8 PFSAs** (PFBS, PFHxS PFOS)	212 ng L^{-1} 133 ng L^{-1} 109 ng L^{-1} 24 ng L^{-1} 430 ng L^{-1} <1 ng L^{-1} 1 ng L^{-1} <1 ng L^{-1} <1 ng L^{-1} 171 ng L^{-1} 13 ng L^{-1} 27 ng L^{-1} **Real** (Mix)	**AE resin** (A600E Polystyrene-DVB gel-type Trimethyl quaternary amine A520E Polystyrene-DVB macroporous-type Trimethyl quaternary amine A532E Polystyrene-DVB gel-type Bifunctional quaternary amine)	10.1 min	**DOM** (GW)	n.a.	Column Pilot-scale	Effect of OM has not been assessed.	(Zaggia et al., 2016)
		GAC C (mesh: 8x30, iodine number 900 mg g^{-1}) J (mesh: 12x40, iodine number 1100 mg g^{-1}) S (mesh: 12x40, iodine number 1000 mg g^{-1})	10 – 11 min			Column Full-scale		
PFBA **PFOA**	1 µg L^{-1} **Spiking** (Single compound)	**Biochar** (HWC, PWC)	50 mg in 150 mL 333 mg L^{-1} 1:3 mg mL^{-1} (biochar:PFAA volume ratio)	**EfOM** (Tertiary treated WW effluent)	DOC = 4.9 mg L^{-1}	Batch adsorption kinetic tests, samples are continuously mixed over 30 days on an orbital shaker	Slow kinetics for PFBA and PFOA adsorption may be attributed to pre-loaded EfOM on the biochar surface. At the equilibrium, the amount of PFOA adsorbed is 3-4 times higher than the amount of PFBA sorbed on both HWC and PWC.	(Inyang and Dickenson, 2017)
PFOA	0.01 – 100000 µg L^{-1} **Spiking**	**Biochar** (HWC, PWC)	1:3 mg mL^{-1} (biochar:PFAA volume ratio)	**EfOM** (Tertiary treated WW effluent) **NOM** (LW, Lake Mead in Southern Nevada)	DOC = 4.9 mg L^{-1} DOC = 2.0 mg L^{-1}	Batch adsorption isotherm tests using two test waters for evaluating the impact of source water on the adsorption of PFOA on different type of biochar	Effect of OM on PFOA adsorption is more intense in WW in which the higher DOC concentration has been measured. OM molecules occupy high-energy pore sites and consequently they lead to pore blockage during PFOA adsorption. OM adsorbed leads also to a change in surface charge with the increasing of repulsion forces between anionic PFOA molecules and biochar surfaces. PFOA adsorbed in WW is 25% less than that in LW.	

Table 4 Experimental studies (both batch and column test) of PFAS adsorption performed in the presence of organic matter (continued).

Adsorbate		Adsorbent		Organic matter		Experimental setup	Remarks	References
Target PFAS	**Level**	**Type**	**Batch dose or EBCT**	**Source (Water matrix)**	**Concentration**			
PFPeA **PFHxA** **PFOA** **PFOS**	17.6 ± 2.4 ng L^{-1} 9.5 ± 1.4 ng L^{-1} 7.3 ± 0.8 ng L^{-1} 4.1 ± 5.6 ng L^{-1} **Real** (Mix)	**GAC** (Norit 830) **Anthracite** (Leopold) **Biochar** (HWC)	8 min	**EfOM** (Tertiary treated WW effluent)	DOC = 4.9 mg L^{-1}	Column Pilot-scale	Faster breakthrough for PFAS tested is observed in anthracite and biochar filters than GAC. The latter shows the best PFAS removal efficiency in comparison with anthracite and HWC. Effect of OM has not been highlighted.	(Inyang and Dickenson, 2017)
PFBS **PFHpA** **PFNA** **PFOA**	32 ng L^{-1} 27 ng L^{-1} 7 ng L^{-1} 26 ng L^{-1}	**Biofilter** (O_3 + GAC)	23 min	**DOM** (water reclamation plant)	DOC = 4.17 mg L^{-1}	Column Pilot-scale	In the pre-ozonated regenerated GAC biofilter more active sites are accessible for PFAS, due to the oxidation of competitive organic compounds. However, short-chain PFAS adsorption amount is lower than long-chain ones.	(Sun et al., 2018)
C_4 – C_{13} PFCAs (PFBA, PFPeA PFHxA, PFHpA, PFOA, PFNA, PFDA, PFDoDA, PFTrDA) **C_4 – C_{10} PFSAs** (PFBS, PFPeS, PFHxS, PFHpS, PFOS, PFNS, PFDS)	1 µg L^{-1} of each compound **Spiking** (Mix)	**PEI-f-CMC**	25 mg L^{-1}	**DOM** (LW)	DOC = 2 mg L^{-1} $SUVA_{254}$ = 2.0 L mg^{-1} m^{-1}	Batch	The longest PFAS (PFDoDA, PFTrDA, PFNS, PFDS) are better removed in lake water than in DI (removal efficiency is ~100% and ~85%, respectively). Whereas, the removal efficiency of short PFCAs is higher in DI (<20%). Removal efficiency of others PFAS is almost equal in both LW and DI.	(Ateia et al., 2018)
				Isolated NOM (hydrophobic type)	DOC = 2.5 mg L^{-1} $SUVA_{254}$ = 4.9 L mg^{-1} m^{-1}		The removal efficiency of short-chain PFAS is higher at the highest $SUVA_{254}$ (hydrophobic NOM). However, short-chain PFAS removal efficiency is lower than 30%. The difference in NOM composition (different $SUVA_{254}$) does not influence the adsorption of longer PFAS, whose removal efficiency is higher than 70%.	
				Isolated NOM (hydrophilic type)	DOC = 2.5 mg L^{-1} $SUVA_{254}$ = 1.7 L mg^{-1} m^{-1}			

EBCT: Empty bed contact time; PAC: powdered activated carbon; EfOM: effluent organic matter; DOC: dissolved organic carbon; GAC: granular activated carbon; DOM: dissolved organic matter; SW: Surface water; RSSCT: rapid small-scale column tests; MWCNTs: multi-walled carbon nanotubes; HA: humic acids; R-CAC: reactivated coconut shell based GAC; EWTP: electroplating wastewater treatment plant; TOC: total organic carbon; DW: drinking water; FA: fulvic acids; AE: anion-exchange; GW: groundwater; LW: lake water; NOM: natural organic matter; DI: deionized water; WWTP: wastewater treatment plant; TCE: tri- chloroethylene; MB: methylbenzene; SDS: sodium dodecyl sulphate; ACF: activated carbon fiber; BdAC: bamboo-derived AC; PFSOF WWW: perfluorooctanesulfonyl fluoride washing wastewater; DFB-CDP : cross-linked polymer network where β-CD substitutes decafluorobiphenyl; BSA: bovine serum albumin; F-MT: Fluorinated montmorillonite; HDPE: high-density polyethylene; PS: polystyrene; PS-COOH: poly-styrene carboxylic acid; RW: river water; SeaW: seawater; MNPs@FG: magnetic nano-particles attached into fluorographene; AFFF: Aqueous film-forming foam; CTF: Covalent triazine-based framework; SWNT: single-walled carbon nanotubes; HWC: hardwood biochar; PWC: pinewood biochar; PEI-f-CMC: poly(ethylenimine)-functionalized cellulose microcrystals; $SUVA_{254}$: specific ultra-violet absorbance at 254 nm.

Table 5 Chemical regeneration of PFAS-saturated materials.

Adsorbate	Adsorbent	Water matrix in adsorption experiments	Ratio mass:solution mixture	Experimental setup	Chemical solution	Regeneration percentage (%)	References
PFOS	**PAC** hydrophobic surface S_{BET} = 980 m^2 g^{-1} pore volume = 276 mm^3 g^{-1}	DI	100 mg:50 mL	Batch Adsorbed PFOS is extracted by varying ethanol and Milli-Q water ratios T=25 °C	100% C_2H_5OH	75.41	(Punyapalakul et al., 2013)
					70% C_2H_5OH + 30% DI	87.41	
					50% C_2H_5OH + 50% DI	94.58	
					40% C_2H_5OH + 60% DI	81.46	
					30% C_2H_5OH + 70% DI	80.96	
					20% C_2H_5OH + 80% DI	55.16	
					10% C_2H_5OH + 90% DI	45.22	
	HMS hydrophilic surface S_{BET} = 712 m^2 g^{-1} pore volume = 773 mm^3 g^{-1}				100% C_2H_5OH	101.27	
					70% C_2H_5OH + 30% DI	101.14	
					50% C_2H_5OH + 50% DI	100.16	
					40% C_2H_5OH + 60% DI	74.74	
					30% C_2H_5OH + 70% DI	71.50	
					20% C_2H_5OH + 80% DI	68.47	
					10% C_2H_5OH + 90% DI	58.69	
	OD-HMS hydrophobic surface S_{BET} = 476 m^2 g^{-1} pore volume = 499 mm^3 g^{-1}				100% C_2H_5OH	101.12	
					70% C_2H_5OH + 30% DI	100.72	
					50% C_2H_5OH + 50% DI	101.34	
					40% C_2H_5OH + 60% DI	61.70	
					30% C_2H_5OH + 70% DI	66.07	
					20% C_2H_5OH + 80% DI	60.98	
					10% C_2H_5OH + 90% DI	57.90	
PFOA	**Purosorb PAD 500** Polysyrenic macroporous-type, nonionic Exchange capacity = n.a.	DI	5 g:250 mL	Batch, magnetic stirrer at 250 rpm in a thermostatic oven for 80 h T=20 °C	5% NH_4Cl	0	(Conte et al., 2015)
					5% NH_4OH	0	
					3% NH_4Cl + 3% NH_4OH	0	
					30% MeOH	20	
					50% MeOH + 3% NH_4OH	90	
	Macronet MN102 Polystyrenic crosslinked macroporous-type, tertiary amine functional groups Exchange capacity = 0.2 meq L^{-1}				5% NH_4Cl	0	
					5% NH_4OH	0	
					3% NH_4Cl + 3% NH_4OH	0	
					30% MeOH	20	
					50% MeOH + 3% NH_4OH	90	
	AE resin **Purolite A600E** Polystyrenic gel-type, quaternary ammonium with trimethyl group functional groups Exchange capacity = 1.4 meq L^{-1}				5% NH_4Cl	20	
					5% NH_4OH	30	
					3% NH_4Cl + 3% NH_4OH	85	
					30% MeOH	< 20	
					50% MeOH + 3% NH_4OH	40	
	AE resin **Purolite A520E** Polystyrenic macroporous-type, quaternary ammonium with trimethyl group functional groups Exchange capacity = 0.9 meq L^{-1}				5% NH_4Cl	35	
					5% NH_4OH	35	
					3% NH_4Cl + 3% NH_4OH	90	
					30% MeOH	20	
					50% MeOH + 3% NH_4OH	50	

* After 5 **Adsorption**/regeneration cycles.
PAC: powdered activated carbon; S_{BET}: BET surface area; DI: deionized water; HMS: hexagonal mesoporous silica; OD-HMS: N-octyldichlorosilane grafted hexagonal mesoporous silica; AE: anion-exchange;

Table 5 Chemical regeneration of PFAS-saturated materials (continued).

Adsorbate	Adsorbent	Water matrix in adsorption experiments	Ratio mass:solution mixture	Experimental setup	Chemical solution	Regeneration percentage (%)	References
PFOS	**BdAC** S_{BET} = 2450 m^2 g^{-1} Effective size = 0.6–0.85 mm	DI	10 g:100 mL	Batch, orbital shaker at 175 rpm for 24 h T = 25 °C	DI	19.8	(Deng et al., 2015b)
					50% CH_3OH	93	
					50% C_2H_5OH	98	
				Batch, orbital shaker at 175 rpm for 7 h T = 80 °C	DI	53	
				Batch, orbital shaker at 175 rpm for 24 h	0.06% NaCl	< 1	
					0.06% NaOH		
				Batch, orbital shaker at 175 rpm for 23 h T = 45 °C	40% C_2H_5OH	89	
					10% C_2H_5OH	46	
					20% C_2H_5OH	71	
					30% C_2H_5OH	80	
				Batch, orbital shaker at 175 rpm for 12 h T = 25 °C	50% C_2H_5OH	70 *	
PFOA	**BdAC** S_{BET} = 2450 m^2 g^{-1} Effective size = 0.6–0.85 mm	Actual WW	25 g:30 mL	Batch, spent adsorbents shake at a thermostatic shaker at 170 rpm for 12 h T = 45 °C	50% CH_3OH	60 *	(Du et al., 2015)
PFHpA						< 30 *	
PFHxA						< 10 *	
PFOA	**AE resin** **Amberlite IRA-67** Acrylic gel-type, tertiary amine functional groups Exchange capacity = 1.6 meq mL^{-1}		10 g:30 mL	Batch, spent adsorbents shake at a thermostatic shaker at 170 rpm for 12 h T = 25 °C	1% NaCl/CH_3OH	< 80 *	
PFHpA						< 40 *	
PFHxA						< 10 *	
PFBA **PFOA** **PFBS** **PFOS**	**AE resin** **Purolite A600E** Polystyrene-DVB gel-type, trimethyl quaternary amine functional groups Exchange capacity = 1.6 eq L^{-1}	DW	1 g:1 L	Batch, flash stirred for 18 h and later at controlled temperature for 60 h T= 20 °C	5% NaCl	0	(Zaggia et al., 2016)
					5% KCl		
					5% NH_4Cl	0 - 5	
					2% NaOH		
					2% KOH		
					2% NH_4OH		
					0.5% NaOH + 0.5% NaCl	< 10	
					0.5% KOH + 0.5% KCl	40 - 60	
					0.5% NH_4OH + 0.5% NH_4Cl		
					80% CH_3OH + 1% NH_4Cl	60 - 80	
					80% CH_3CH_2OH + 1% NH_4Cl		
	AE resin **Purolite A520E** Polystyrene-DVB macroporous-type, trimethyl quaternary amine functional groups Exchange capacity = 0.9 eq L^{-1}	DW			5% NaCl	0	
					5% KCl		
					5% NH_4Cl	< 10	
					2% NaOH	0 - 5	
					2% KOH		
					2% NH_4OH	< 10	

* After 5 **adsorption**/regeneration cycles.
BdAC: bamboo-derived activated carbon; S_{BET} = BET surface area; AE: anion-exchange; WW: wastewater; DW: drinking water; DI: deionized water.

Table 5 Chemical regeneration of PFAS-saturated materials (continued).

Adsorbate	Adsorbent	Water matrix in adsorption experiments	Ratio mass:solution mixture	Experimental setup	Chemical solution	Regeneration percentage (%)	References
PFOS	**Chitosan-based MIP**	DI	0.01 g:100 mL	Batch regeneration solution in an orbital shaker for 24 h T = 40 °C	90% NaOH + 10% C_3H_6O	60 *	(Yu et al., 2008)
PFOS	**AE resin** **Amberlite IRA-458** Acrylic gel-type, quaternary ammonium functional groups Exchange capacity = 1.25 meq mL^{-1}	DI	n.a.	Column Resin loaded with PFOS or PFBS packed in glass column (diameter of 1 cm, height of 10 cm) Flow rate 20 mL/min for 12 h T=22 °C	NaCl (320 mM)	0.0	(Carter and Farrell, 2010)
					NaOH (320 mM)	0.36	
PFBS					NaOH (320 mM)	4	
PFOS	**AE resin** **Amberlite IRA-958** Acrylic macroreticular-type, quaternary ammonium functional groups Exchange capacity = 0.8 eq L^{-1}	Chromium planting WW (inorganic anions)	20 mg:100 mL	Batch Resin loaded with PFOS and regeneration solution in an orbital shaker for 24 h at 150 rpm T = 25 °C	5% NaCl	< 10	(Deng et al., 2010)
					5% NaCl + 10% CH_3OH		
					1% NaCl + 10% CH_3OH		
					1% NaCl + 30% CH_3OH		
					100% CH_3OH		
					4% NaOH		
					1% NaCl + 50% CH_3OH	70	
					1% NaCl + 50% CH_3OH	90	
	AE resin **Amberlite IRA-67** Acrylic gel-type, tertiary amine functional groups Exchange capacity = 1.6 meq mL^{-1}				100% CH_3OH	< 5	
					4% NaOH	< 5	
					0.4% NaOH	45	
					0.04% NaOH	50	
					1% NaCl + 30% CH_3OH	20	
					1% NaCl + 50% CH_3OH	85	
					1% NaCl + 70% CH_3OH	95	
					1% NaOH + 30% CH_3OH	95	
					1% NaOH + 50% CH_3OH	90	
					1% NaOH + 70% CH_3OH	90	

* After 5 **adsorption**/regeneration cycles.
MIP: molecularly imprinted; AE: Anion-exchange; WW: wastewater; DW: drinking water; DI: deionized water.

Table 5 Chemical regeneration of PFAS-saturated materials (continued).

Adsorbate	Adsorbent	Water matrix in adsorption experiments	Ratio mass:solution mixture	Experimental setup	Chemical solution	Regeneration percentage (%)	References
PFBA PFOA PFBS PFOS	**AE resin Purolite A520E** Polystyrene-DVB macroporous-type, trimethyl quaternary amine functional groups Exchange capacity = 0.9 eq L^{-1}	DW	1 g:1 L	Batch, flash stirred for 18 h and later at controlled temperature for 60 h T = 20 °C	0.5% NaOH + 0.5% NaCl	10 - 20	(Zaggia et al., 2016)
					0.5% KOH + 0.5% KCl	50 - 65	
					0.5% NH_4OH + 0.5% NH_4Cl	70 - 80	
					80% CH_3OH + 1% NH_4Cl	80 - 90	
					80% CH_3CH_2OH + 1% NH_4Cl		
					5% KCl		
	AE resin Purolite A532E Polystyrenic macroporous-type, bifunctional quaternary amine functional groups Exchange capacity = 0.85 eq L^{-1}	DW	1 g:1 L	Batch, flash stirred for 18 h and later at controlled temperature for 60 h T = 20 °C	5% NaCl	0	
					5% KCl		
					5% NH_4Cl	0 - 5	
					2% NaOH	0	
					2% KOH		
					2% NH_4OH	0 - 5	
					0.5% NaOH + 0.5% NaCl		
					0.5% KOH + 0.5% KCl		
					0.5% NH_4OH + 0.5% NH_4Cl		
					80% CH_3OH + 1% NH_4Cl	80 - 90	
					80% CH_3CH_2OH + 1% NH_4Cl		
PFOS	**R-CAC** S_{BET} = 1750 m^2 g^{-1}	Actual WW	10mg:20 mL	Batch, shaking at 170 rpm for 12 h T = 50 °C	50% C_2H_5OH	76.0	(Du et al., 2016a)
					70% C_2H_5OH	89.5	
					90% C_2H_5OH	85.1	
					100% C_2H_5OH	83.1	
				Batch, shaking at 170 rpm for 12 h T = 40 °C	50% CH_3OH	85.3	
					70% CH_3OH	89.5	
					90% CH_3OH	95.1	
					100% CH_3OH	90.2	
					50% C_3H_6O	80.6	
					70% C_3H_6O	85.6	
					90% C_3H_6O	91.6	
					100% C_3H_6O	90.0	
F-53B	**R-CAC** S_{BET} = 1750 m^2 g^{-1}	Actual WW	10mg:20 mL	Batch, shaking at 170 rpm for 12 h T = 50 °C	50% C_2H_5OH	80.4	
					70% C_2H_5OH	96.6	
					90% C_2H_5OH	90.2	
					100% C_2H_5OH	88.3	
				Batch, shaking at 170 rpm for 12 h T = 40 °C	50% CH_3OH	88.3	
					70% CH_3OH	93.1	
					90% CH_3OH	97.7	
					100% CH_3OH	92.6	
					50% C_3H_6O	87.4	
					70% C_3H_6O	92.3	
					90% C_3H_6O	97.6	
					100% C_3H_6O	93.4	

AE: anion-exchange; WW: wastewater; DW: drinking water; DI: deionized water; R-CAC: reactivated coconut shell based GAC; S_{BET} = BET surface area.

Table 5 Chemical regeneration of PFAS-saturated materials (continued).

Adsorbate	Adsorbent	Water matrix in adsorption experiments	Ratio mass:solution mixture	Experimental setup	Chemical solution	Regeneration percentage (%)	References
PFOS **PFHxS** **PFBS**	**PCMAs**	DI	0.5 g/L of PCMAs with 50 mg/L of each PFAS	Adsorbed PFAS are extracted with methanol. Regenerated PCMAs are reused for subsequent PFAS sorption experiments.	CH_3OH	85 - 88 *	(Wang et al., 2014)
PFOS	**PACFs**	DI	10mg:100 mL	Batch, shaking at 180 rpm for 24 h T = 25 °C	DI	5	(Chen et al., 2017)
					10% C_2H_5OH	22	
					30% C_2H_5OH	65	
					50% C_2H_5OH	85	
					100% C_2H_5OH	87	

* After 5 adsorption/regeneration cycles
DI: deionized water; PCMAs: permanently confined micelle arrays; PACFs: Polyacrylonitrile fiber (PANF)-derived activated carbon fibers

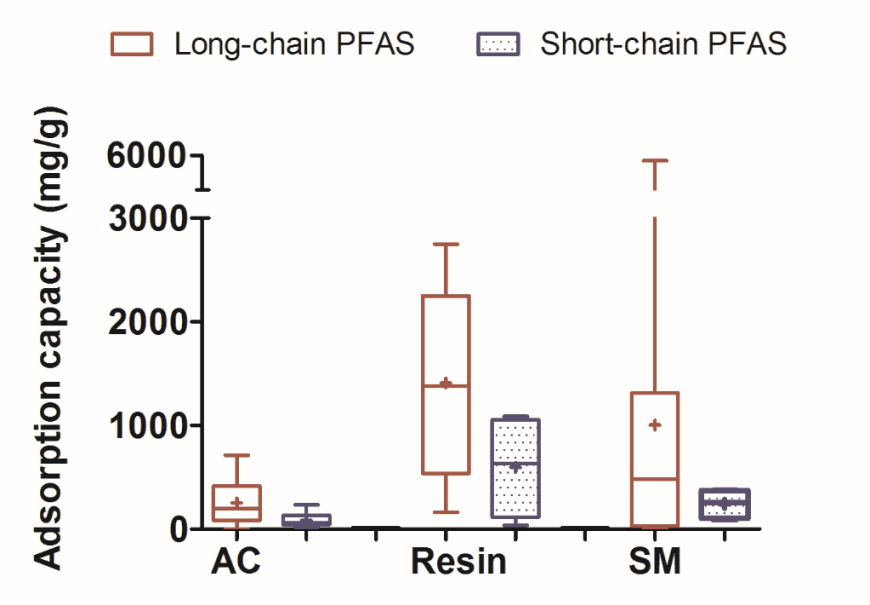

Figure 1 Box-and-whiskers plot concerning the adsorption capacity of long- and short-chain PFAS on different adsorbent materials (AC: activated carbon; Resin; SM: Synthetized materials).

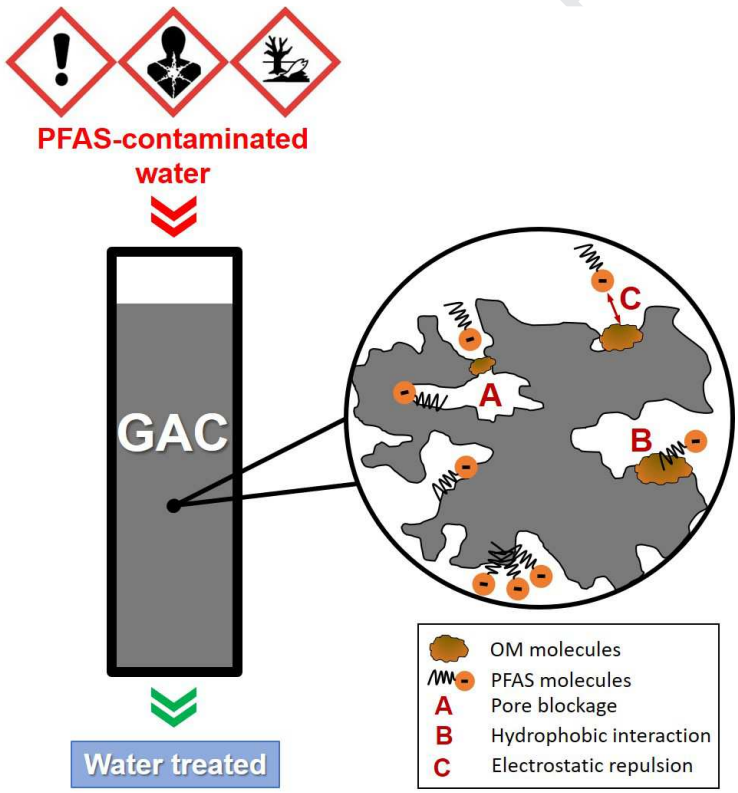

Figure 2 The main interactions established between OM and PFAS molecules during GAC adsorption. A: pore blockage; B: hydrophobic interaction; C: electrostatic repulsion.

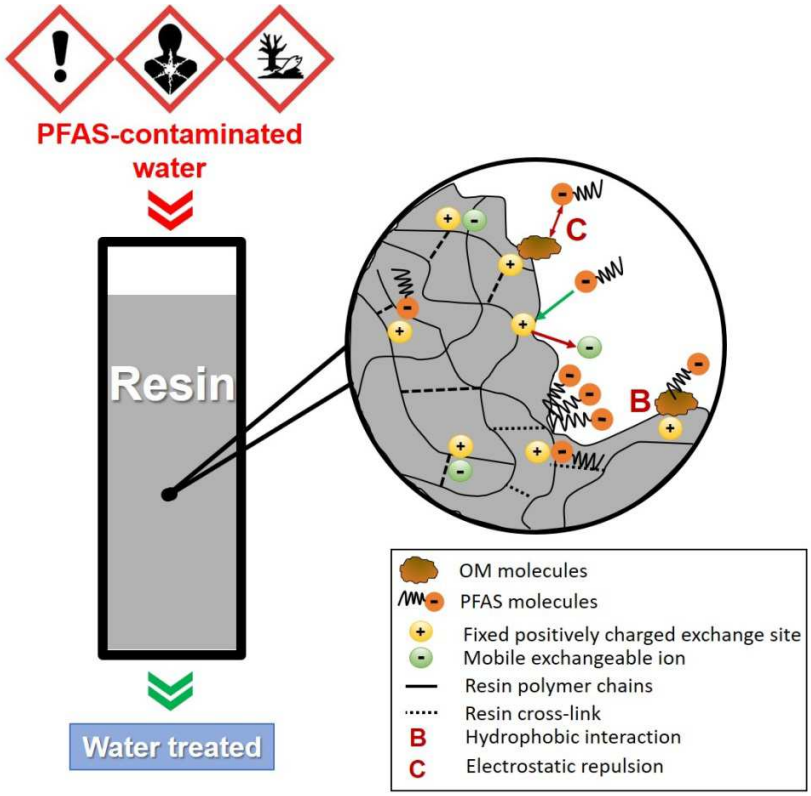

Figure 3 The main interactions established between OM and PFAS molecules during anion-exchange process. B: Hydrophobic interaction; C: Electrostatic repulsion.

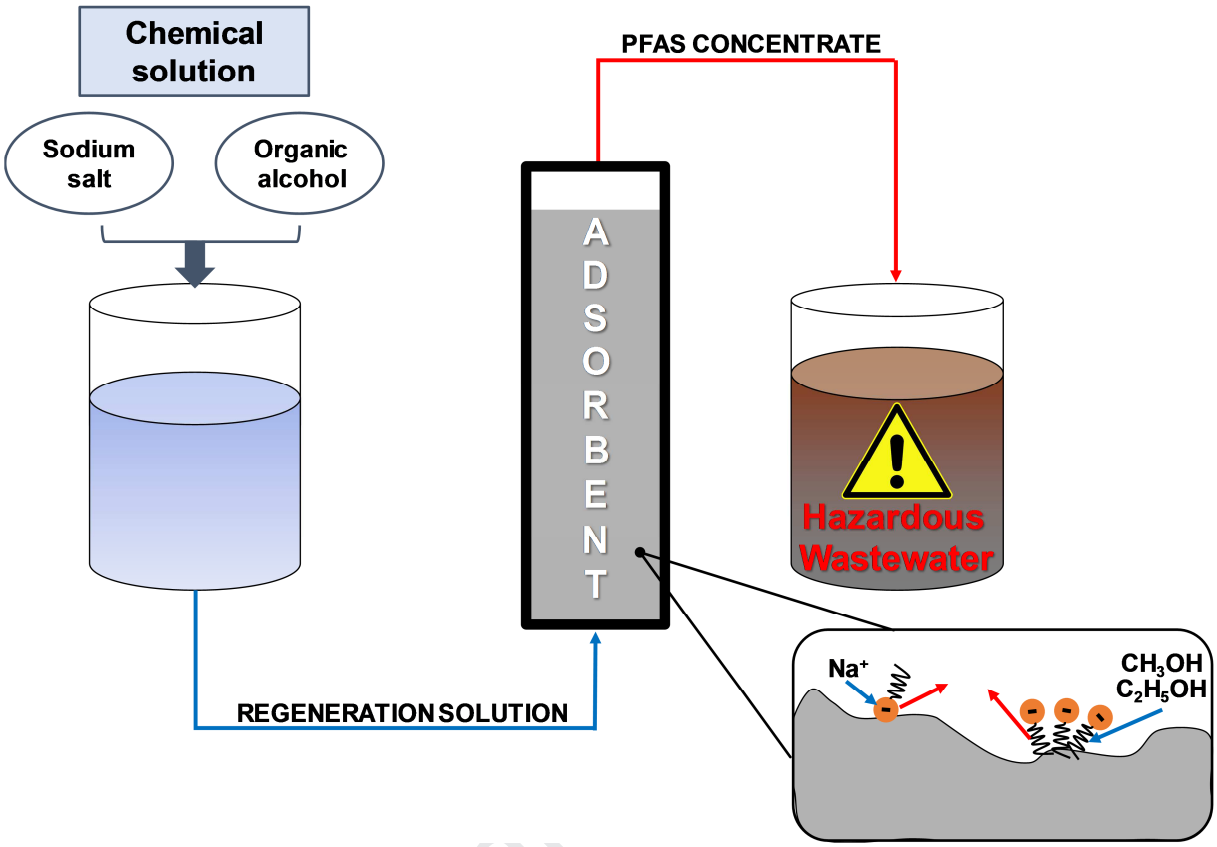

Figure 4 Chemical regeneration of PFAS-exhausted adsorbents using a solution of sodium salt and organic alcohol.

Highlights

- Most PFAS adsorption studies were carried out under unrealistic conditions.
- Organic matter often improves long-chain PFAS adsorption by aggregates formation.
- Co-existing OM reduces the short-chain PFAS adsorption efficiency.
- Short-chain PFAS are better removed by anion-exchange mechanism.
- Regeneration of PFAS-saturated adsorbents often needs harmful organic solvents.

Declaration of interests

☒ The authors declare that they have no known competing financial interests or personal relationships that could have appeared to influence the work reported in this paper.

☐The authors declare the following financial interests/personal relationships which may be considered as potential competing interests: